SANDIA REPORT

SAND2004--5878
Unlimited Release
Printed November 2004

Multi-dimensional Modeling of Atmospheric Copper-Sulfidation Corrosion on non-Planar Substrates

Ken S. Chen

Prepared by
Sandia National Laboratories
Albuquerque, New Mexico 87185 and Livermore, California 94550

Sandia is a multiprogram laboratory operated by Sandia Corporation,
a Lockheed Martin Company, for the United States Department of Energy's
National Nuclear Security Administration under Contract DE-AC04-94AL85000.

Issued by Sandia National Laboratories, operated for the United States Department of Energy by Sandia Corporation.

Available to DOE and DOE contractors from
U.S. Department of Energy
Office of Scientific and Technical Information
P.O. Box 62
Oak Ridge, TN 37831

Telephone: (865)576-8401
Facsimile: (865)576-5728
E-Mail: reports@adonis.osti.gov
Online ordering: http://www.osti.gov/bridge

Available to the public from
U.S. Department of Commerce
National Technical Information Service
5285 Port Royal Rd
Springfield, VA 22161

Telephone: (800)553-6847
Facsimile: (703)605-6900
E-Mail: orders@ntis.fedworld.gov
Online order: http://www.ntis.gov/help/ordermethods.asp?loc=7-4-0#online

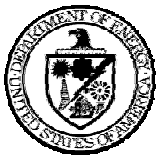

SAND 2004-5878
Unlimited Release
Printed November 2004

Multi-dimensional Modeling of Atmospheric Copper-Sulfidation Corrosion on non-Planar Substrates

Ken S. Chen

Multiphase Transport Processes Department
Sandia National Laboratories
P.O. Box 5800
Albuquerque, New Mexico 87185-0834

Abstract

This report documents the author's efforts in the deterministic modeling of copper-sulfidation corrosion on non-planar substrates such as diodes and electrical connectors. A new framework based on Goma was developed for multi-dimensional modeling of atmospheric copper-sulfidation corrosion on non-planar substrates. In this framework, the moving sulfidation front is explicitly tracked by treating the finite-element mesh as a pseudo solid with an arbitrary Lagrangian-Eulerian formulation and repeatedly performing re-meshing using CUBIT and re-mapping using MAPVAR. Three one-dimensional studies were performed for verifying the framework in asymptotic regimes. Limited model validation was also carried out by comparing computed copper-sulfide thickness with experimental data. The framework was first demonstrated in modeling one-dimensional copper sulfidation with charge separation. It was found that both the thickness of the space-charge layers and the electrical potential at the sulfidation surface decrease rapidly as the Cu_2S layer thickens initially but eventually reach equilibrium values as Cu_2S layer becomes sufficiently thick; it was also found that electroneutrality is a reasonable approximation and that the electro-migration flux may be estimated by using the equilibrium potential difference between the sulfidation and annihilation surfaces when the Cu_2S layer is sufficiently thick. The framework was then employed to model copper sulfidation in the solid-state-diffusion controlled regime (i.e. stage II sulfidation) on a prototypical diode until a continuous Cu_2S film was formed on the diode surface. The framework was also applied to model copper sulfidation on an intermittent electrical contact between a gold-plated copper pin and gold-plated copper pad; the presence of Cu_2S was found to raise the effective electrical resistance drastically. Lastly, future research needs in modeling atmospheric copper sulfidation are discussed.

Acknowledgment

This work was funded by the Accelerated Scientific Computing program and has benefited from the numerous interactions within Sandia's Corrosion Initiative spearheaded by Jeff Braithwaite. In particular, the author would like to knowledge the helpful interactions/discussions with Charles Barbour, Jeff Braithwaite, Michael Campin, David Enos, Rich Larson, Harry Moffat, Rob Sorensen, and Amy Sun during the course of this work. The author would also like to thank Harry Moffat and Amy Sun for careful reviews of the manuscript and helpful comments.

Contents

1. Introduction

Copper-containing electrical and electronic devices (e.g., diodes, electrical interconnects) can corrode to form corrosion products (e.g., copper sulfide) in the presence of a corroding atmosphere containing hydrogen sulfide (H_2S) and oxygen with some level of humidity (see e.g., Sorensen et al. 1996, Sorensen et al. 2001, Braithwaite et al. 2003). Figure 1 shows examples of atmospheric corrosion observed in fielded copper-containing components (Braithwaite et al. 2003, Moffat et al. 2000). Hydrogen sulfide is a product of the anaerobic degradation of organic sulfur compounds (Leygraf and Graedel 2000); it may also be generated from the decomposition of sulfur-containing parts (e.g., rubber seal rings) nearby or surrounding the electrical and electronic devices. Formation of copper sulfide (Cu_2S) corrosion product, which occurs in a process called copper sulfidation, can have detrimental effects or even cause malfunctions of copper-containing components. For example, a continuous Cu_2S film formed on the surface of a diode can conduct leakage electrical current, which in turn can cause the diode to malfunction when the leakage current is sufficiently high. Cu_2S formed on an electrical contact can raise the effective electrical resistance such that electrical current conducted through the contact under constant voltage will be reduced to an unacceptably low level so as to render contact failure. In short, understanding the mechanisms involved in copper-sulfidation corrosion and being able to predict the rates of copper sulfidation for given environmental conditions will be valuable in stockpile stewardship.

Due to its importance, atmospheric copper-sulfidation corrosion has attracted considerable interests from inside and outside Sandia, and numerous studies have been carried out. Graedel and his collaborators at AT&T (now Lucent Technologies) Bell Laboratories have pioneered the studies of atmospheric copper sulfidation corrosion (see, e.g., Graedel et al. 1983, Graedel et al. 1985, Graedel et al. 1987, Graedel 1996, Tidblad and Graedel 1996) in both experimental investigation and physical or mechanistic model development. The textbook of Leygraf and Graedel (2000) summarizes the research work on atmospheric copper-sulfidation corrosion conducted at the Royal Institute of Technology, Stockholm, Sweden and at AT&T Bell Laboratories.

Atmospheric sulfidation of a diode has been first studied experimentally at Sandia by Sorensen and Braithwaite and their collaborators (Sorensen et al. 1996, Krska et al. 1996). An experimental study on the atmospheric degradation of gold- and nickel-gold-electroplated copper connectors was carried out by Enos et al. (2003). The mechanisms of atmospheric copper sulfidation were investigated by Barbour et al. (2002) using parallel and conventional experimentation. The effect of gas-phase mass transport on atmospheric copper sulfidation was studied by Braithwaite et al. (2000) whereas the effect of humidity on atmospheric copper-sulfidation kinetics was examined by Enos et al. (2002). Studies on the effects of varying humidity on copper sulfidation, in particular on the microstructure or morphology of the Cu_2S corrosion product, were carried out by Sullivan et al. (2004) and Campin (2003). A long time (77 days) exposure test on the atmospheric corrosion of copper by hydrogen sulfide in underground condition was conducted by Tran et al. (2003) who show that exposure tests performed for short times in synthetic atmospheres cannot be extrapolated to long time exposure in real conditions.

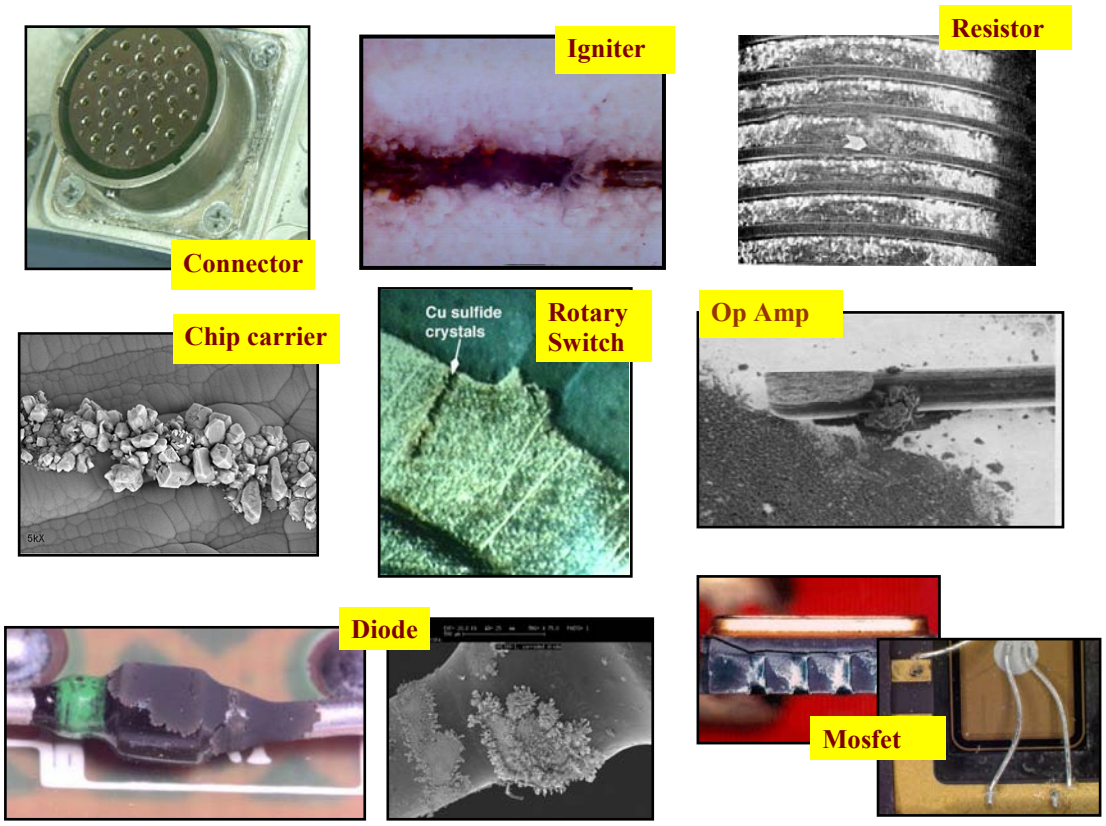

Figure 1. Examples of atmospheric corrosion observed in fielded copper-containing components (Braithwaite et al. 2003, Moffat et al. 2000)

Larson (1998) made his first attempt at modeling the atmospheric sulfidation of copper by proposing a physical copper-sulfidation model that includes four distinct phases: the substrate metal, a cohensive cuprous sulfide (Cu_2S) product layer, a thin aqueous film adsorbed on the sulfide, and the ambient gas. Larson's four-phase physical model is much simpler than the six-regime GILDES model previously proposed by Graedel (1996), which refers to Gas, the Interface between gas and liquid, the Liquid, the Deposition layer, the Electrodic region near the surface (for conducting and semiconducting solids), and the Solid. Larson further postulated that transport through the sulfide layer occurs via diffusion and electromigration of copper vacancies and electron holes. Larson solved the pseudo-steady state, one-dimensional governing equations (which describe the copper sulfidation process based the physical model that he developed) numerically by employing the standard SLATEC routine DNSQE and a shooting method coupled with DASSL (a stiff ODE solver). Subsequently, Larson (2002) refined the copper-sulfidation model he developed previously by focusing on the transport of charged lattice defects in a growing Cu_2S product layer between the ambient gas and the substrate metal. As previously, this transport is postulated to occur via both diffusion and electromigration. Unlike the previous model, however, the vacancy and hole annihilation reaction is taken to take place at the copper/sulfide interface whereas the copper-sulfidation reaction is assumed to occur at the sulfide/gas interface. Besides solving the governing equations in one-dimension numerically as previously, Larson also obtained analytical solution for the asymptotic limit

of thick sulfide layer and found that the assumption of electroneutrality in the sulfide (which can drastically simplify the numerical computations) gives rise to very little error under typical conditions.

A multi-length-scale (from atomistic subgrid to multi-dimensional multi-phase continuum) and multi-disciplinary approach was presented by Moffat et al. (2000) for modeling atmospheric sulfidation of copper. Sandia's efforts in developing an analytical capability for predicting the effect of corrosion on the performance of electrical components were reported by Sorensen et al. (2001) and Braithwaite et al. (2003). The efforts of multi-dimensional modeling of atmospheric copper sulfidation on non-planar substrates such as diodes and electrical connectors were presented by Chen (2003) and are documented in this report. Portions of this report has been reported/documented in conference papers and Sandia memoranda or reports (Chen 1999; Chen 2000a, 2000b; Sorensen et al. 2001; Chen 2002a, 2002b; Braithwaite et al. 2003; Chen 2003a, 2003b).

Other efforts, taken place or ongoing, include: 1) parameter estimation for an atmospheric copper-sulfidation corrosion model by DAKOTA (Design Analysis Kit for Optimization and Terascale Application), which was carried out by Sun and Moffat (2003); 2) uncertainty quantification of an atmospheric corrosion model, which was performed by Sun and Moffat (2004); and 3) model development for pore corrosion of noble-metal plated electrical connectors, which were reported most recently by Moffat and Sun (2004a, 2004b & 2004c).

2. Simplified Physical Model

In the present work, the essential phenomena involved in atmospheric copper sulfidation were taken to occur according to the following simplified physical model (cf. Larson 2002, Chen 2002a & 2003b). As depicted in Figure 2, corrodant, H_2S, diffuses from the humidified atmosphere to the surface of the copper substrate initially and the Cu_2S/air interface subsequently. Simultaneously, copper vacancies and electron holes diffuse and migrate within Cu_2S from the stationary Cu/Cu_2S interface to the moving Cu_2S/air interface. Copper vacancies (denoted as V^-) and electron holes (denoted as h^+) are produced at the moving Cu_2S/air interface via the following sulfidation electrochemical reaction in which product water is taken to be liquid (cf. Larson 2002):

$$H_2S(g) + \frac{1}{2}O_2(g) \Leftrightarrow Cu_2S(s) + 2V^- + 2h^+ + H_2O(l) \qquad (1)$$

where *g*, *s*, and *l* within the parentheses denotes gas, solid, and liquid, respectively. Once reaching the Cu/Cu_2S interface, copper vacancies and electron holes are annihilated as follows (cf. Larson 2002):

$$Cu + V^- + h^+ \rightarrow Null \qquad (2).$$

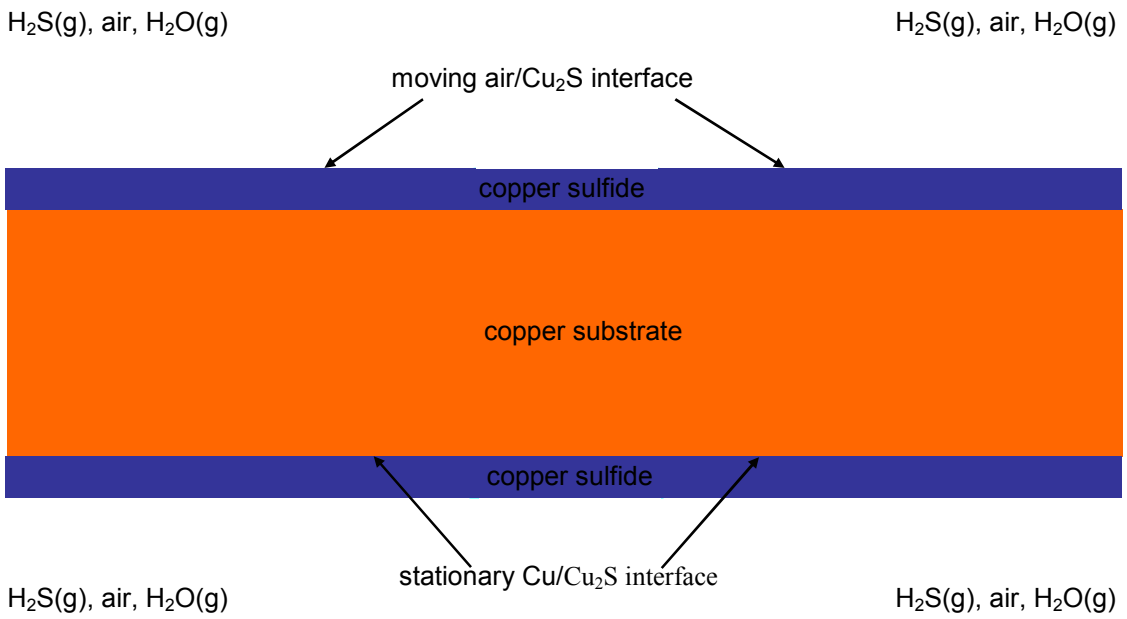

Figure 2. Schematic of a simplified physical model for atmospheric copper sulfidation (not to scale).

Equation 1 represents an overall sulfidation reaction, which involves multiple steps as follow: H_2S gas dissolves into a bulk or thin water layer on the substrate surface, and then dissociates partially as an acid. The process of S^{-2} undergoing oxidation occurs at a slow rate; so slow that it is neglected here. The S^{-2} ions then react with the Cu_2S surface to create an extra lattice site. The reader is referred to Larson (1998)'s SAND report for a proposed mechanism of the full process.

3. Kinetic Rates for the Sulfidation and Annihilation Reactions

Taking the forward and backward reactions in Equation 1 separately as elementary yields the following kinetic rate expression (cf. Braithwaite 2002, Chen 2002a, Larson 2002, Chen 2003b, Sun and Moffat 2003):

$$r_{Cu_2S} = k_1 c_{H_2S} \sqrt{c_{O_2}} - k_{-1} c_{V^-}{}^2 c_{h^+}{}^2 = K_1 c_{H_2S} - k_{-1} c_{V^-}{}^2 c_{h^+}{}^2 \qquad (3)$$

where r_{Cu_2S} is the rate of formation of Cu_2S; k_1 and k_{-1} are the rate constants for, respectively, the forward and backward reactions; c_{H_2S}, c_{O_2}, c_{V^-} and c_{h^+} are concentrations of H_2S, O_2, V^- (copper vacancy in the copper substrate) and h^+ (electron hole) species, respectively; and $K_1 = k_1 \sqrt{c_{O_2}}$ is a constant when both k_1 and c_{O_2} are taken to be constant. Note that concentrations of Cu_2S and H_2O do not appear in the rate expression in Equation

3 since Cu_2S is produced as solid and H_2O is taken to be produced as liquid so that their concentrations are constant. Similarly, regarding the annihilation reaction (Equation 2) as elementary yields (cf. Larson 2002, Chen 2003b):

$$r_{Cu} = k_2 c_{V^-} c_{h^+} \tag{4}$$

where r_{Cu} is the rate of consumption of copper. To account for the temperature effects on the rate constants, k_1, k_{-1} and k_2, the Arrhenius expression can be used (Braithwaite 2002, Chen 2003b):

$$k_1 = k'_1 e^{-\frac{E_1}{RT}} \tag{5},$$

$$k_{-1} = k'_{-1} e^{-\frac{E_{-1}}{RT}} \tag{6},$$

$$k_2 = k'_2 e^{-\frac{E_2}{RT}} \tag{7}.$$

To capture effects of humidity, k'_1, k'_{-1} and k'_2 can further be made functions of humidity.

4. Transport and Kinetic Time Constants

To have an appreciation on the relative time scales of the transport and kinetic processes involved in atmospheric copper sulfidation occurring according to the simplified physical model described above in section 2, it is helpful to estimate the process time constants. The time constant for diffusion, τ_D, can be estimated via the following equation:

$$\tau_D = L^2 / D \tag{8}$$

where L is some characteristic length scale and D is the diffusion coefficient. Since ionic conductivity can be related to diffusivity via the Nernst-Eistein equation, time constant for electro-migration can also be estimated by Equation 8. The time constant for the sulfidation reaction can be estimated by

$$\tau_D = L / K_1 \tag{9}.$$

It is well known that the diffusivity for H_2S diffusion in air, D_{H_2S}, is about 0.1 cm^2/s. Values for D_{V^-} (diffusivity of copper vacancies diffusion in Cu_2S) and K_1, however, are not well known though Larson (2002) found that using $D_{V^-} = 10^{-10}$ cm^2/s and $K_1 = 1.21$ cm/s yields good agreement between Sorensen and Braithwaite's experimental data and his

model predictions. Separately, Moffat (2000) modeled the gas transport in a stagnation point flow reactor that minimizes the gas phase mass transport resistance, and obtained a sticking coefficient of 0.001 for H_2S in Phase I growth of Cu_2S, with a factor of 2 – 4 uncertainty. Using an effusive flux of 10^4 cm/s, this yields $K_1 \approx 10$ cm/s. Table 1 presents time constants for H_2S diffusion in air, copper-vacancy diffusion in Cu_2S, and the copper-sulfidation reaction, respectively using $D_{H_2S} \approx 0.1\ \text{cm}^2/\text{s}$, $D_{V^-} \approx 10^{-10}\ \text{cm}^2/\text{s}$.

Table 1. Transport and Kinetic Time Constants
($D_{H_2S} \approx 0.1\ \text{cm}^2/\text{s}$, $D_{V^-} \approx 10^{-10}\ \text{cm}^2/\text{s}$, and $K_1 \approx 1$ cm/s)

H_2S diffusion in air (0.01cm < L < 1cm)	Copper vacancies diffusion in Cu_2S (10^{-5}cm < L < 0.1cm)	Sulfidation reaction with $K_1 \approx 1$ (10^{-5}cm< L <0.1cm)	Sulfidation reaction with $K_1 \approx 10$ (10^{-5}cm< L <0.1cm)
0.1 s – 10 s	1 s – 10^8 s	10^{-5} s – 0.1 s	10^{-6} s – 10^{-2} s

Obviously, the time constants depend on the characteristic length scale chosen. But it is clear that the time constant for solid-state diffusion of copper vacancies in Cu_2S is much larger than that for gas-phase diffusion of H_2S in air and that for sulfidation reaction. Thus, it can be concluded that copper-vacancy diffusion in Cu_2S is the limiting process that controls the atmospheric copper-sulfidation corrosion. Recently, Campin (2003) has found that grain boundaries significantly interfere with the diffusion of copper vacancies in as-grown materials. D_{V^-} fit to experiments may be significantly affected by the nature and number of grain boundaries. However, the conclusion remains the same – bulk effective diffusion is rate limiting.

5. Governing Equations and Numerical Solution Methods

5.1 Species concentration

The concentrations of H_2S, copper vacancies, and electron holes are governed by the law of species mass conservation:

$$\frac{\partial c_i}{\partial t} + \nabla \cdot J_i = 0 \tag{10}$$

where c_i is concentration of species i, t is time, and J_i is the species flux given by

$$j_i = -D_i \nabla c_i \quad \text{for diffusion of } H_2S \text{ in air} \tag{11},$$

$$j_i = -D_i \nabla c_i - \frac{F}{RT} z_i D_i c_i \nabla \Phi \quad \text{for diffusion and migration of copper vacancies and electron holes in } Cu_2S \tag{12}.$$

In Equations 11 and 12, D_i and z_i are, respectively, diffusivity and charge number of species *i*; *F* is Faraday's constant (≡96487 C/mole) and *R* is the universal gas constant; and Φ is electric potential in Cu_2S arising from the interactions between copper vacancies and electron holes.

5.2 Electric potential in copper sulfide with charge separation

The electric potential in Cu_2S is governed by the law of charge conservation or the well-known *Poisson* equation (cf. Newman 1991, Chen 2002):

$$\nabla^2\Phi = -\frac{F}{\varepsilon}\sum_i z_i c_i = -\frac{F}{\varepsilon}(c_{h^+} - c_{V^-}) \tag{13}$$

where ε is permittivity of Cu_2S in units of *coulomb per volt per unit length* (e.g., C/V-cm or C/V-m). Since the electric filed, *E*, is defined as the negative of the electric potential, i.e., $E = -\nabla\Phi$, Equation 13 can be re-written in terms of electric fielc, *E* (cf. Larson 2002):

$$\nabla E = \frac{F}{\varepsilon}(c_{h^+} - c_{V^-}) \tag{14}$$

where electric field *E* has units of volts per unit length. Since the ratio $\varepsilon/\varepsilon_0$ is called the relative dielectric constant of a solid medium with ε_0 being the permittivity of a vacuum ($\varepsilon_0 \equiv 8.8542\text{x}10^{-14}$ C/V-cm), Equation 14 can be re-written as follows, using the relative dielectric constant of the solid medium, $\kappa(\equiv \varepsilon/\varepsilon_0)$:

$$\nabla E = \frac{F}{\kappa\varepsilon_0}(c_{h^+} - c_{V^-}) \tag{15}.$$

It should be noted that Equation 15 differs from Larson (2002)'s Equation 6, which is due to that $4\pi\varepsilon_0 = 1$ in the *cgs* units (in which electric field has units of *electric static unit per cm*) that Larson has chosen to write the *Poisson* equation; in contrast, electric field *E* in Equation 15 has units of *volts per unit length* (e.g., *V/cm* or *V/m*). In short, Equation 15 above and Equation 6 in Larson (2002)'s paper are consistent but it should be kept in mind that they are written with different units for the electric field. Substituting $\varepsilon = \kappa\varepsilon_0$ in Equation 13 and re-arranging the resultant equation yields:

$$\nabla\cdot(-\kappa\varepsilon_0\nabla\Phi) = F(c_{h^+} - c_{V^-}) = F\sum_{i=1}^{2} z_i c_i \tag{16},$$

which along with Equations 10 and 12 can be solved for Φ, c_{V^-} , and c_{h^+} . Equation 16 was incorporated in Goma by the author using the key word *NET_CHARGE* to specify $F\sum z_i c_i$ as the current source and treating $\kappa\varepsilon_0$ as the electrical conductivity.

In regions or domains in which $c_{V^-} = c_{h^+}$ (i.e. electroneutrality constraint is met), Equation 16 reduces to the familiar Laplace equation:

$$\nabla^2\Phi = 0 \quad \text{or} \quad \nabla\Phi = f(t) \tag{17},$$

which means that the electric-potential gradient is a function of time only (that is, ∇Φ is uniform spatially within the domain in which electroneutrality holds). A simple expression for ∇Φ in 1-D approximation is the following:

$$\nabla\Phi = \frac{d\Phi}{dy} = \frac{\Phi_s - \Phi_a}{h} \tag{18},$$

where *y* is the axis along with copper-vacancy and electron-hole transport; Φ_s and Φ_a are electric potential at the sulfidation and annihilation surfaces, respectively; and *h* is the Cu_2S layer thickness.

5.3 Electric potential in one-dimensional sulfidation with linear copper-vacancy and electron-hole concentrations

For the purpose of verifying Goma (a Sandia-developed finite-element computer code used to solve the governing equations as discussed below in section 5.6) on solving the *Poisson* equation that governs electric potential with charge separation, it is helpful to obtain an analytical solution in some asymptotic regime. Equation 15 when written in one-dimensional (along the Cu_2S layer thickness direction or y-axis) becomes:

$$\frac{dE}{dy} = \frac{F}{\kappa\varepsilon_0}(c_{h^+} - c_{V^-}) \tag{19}.$$

We consider the an asymptotic regime in which the electron-hole and copper-vacancy concentrations can be approximated as linear across the Cu_2S layer and are given by, respectively:

$$c_{h^+}(y) = \left[c_{h^+}(L) - c_{h^+}(0)\right]\frac{y}{L} + c_{h^+}(0) \tag{20},$$

$$c_{V^-}(y) = \left[c_{h^+}(L) + c_{h^+}(0) - 2c_{V^-}(0)\right]\frac{y}{L} + c_{V^-}(0) \tag{21},$$

where L denotes thickness of the Cu_2S layer; $y = 0$ refers to the annihilation surface (i.e., the Cu/Cu_2S interface) and $y = L$ the sulfidation surface. It can be readily shown from Equations 20 and 21 that

$$c_{h^+}(L/2) = c_{V^-}(L/2) \tag{22},$$

and

$$c_{V^-}(L) - c_{h^+}(L) = c_{h^+}(0) - c_{V^-}(0) \tag{23},$$

which are necessary conditions for satisfying the boundary conditions of vanishing electric field at both the annihilation surface ($y = 0$) and the sulfidation surface ($y = L$): $E(0) = E(L) = 0$. Substituting Equations 22 and 23 into Equation 19 and applying the boundary condition of $E(0) = 0$ yields:

$$E(y) = \frac{F}{\kappa\varepsilon_0 L}\left[c_{h^+}(0) - c_{V^-}(0)\right](Ly - y^2) \tag{24}.$$

Equation 24 clearly satisfies the boundary conditions of vanishing electric field at the annihilation and sulfidation surfaces, i.e., $E(0) = 0$ and $E(L) = 0$. Substituting $E = -\nabla\Phi$ into Equation 24 and solving for the electric potential Φ gives:

$$\Phi(y) - \Phi(0) = -\frac{F}{\kappa\varepsilon_0 L}\left[c_{h^+}(0) - c_{V^-}(0)\right]\left(\frac{1}{2}Ly^2 - \frac{1}{3}y^3\right) \tag{25}.$$

The electric potential gradient across the Cu_2S layer in the asymptotic regime of linear copper-vacancy and electron-hole concentrations can easily be determined from Eq. 25:

$$\frac{\Phi(L) - \Phi(0)}{L} = -\frac{FL}{6\kappa\varepsilon_0}\left[c_{h^+}(0) - c_{V^-}(0)\right] \tag{26}.$$

5.4 Mesh nodal displacement

To solve for the nodal displacements of the finite-element mesh (the nodal positions of the mesh need to be solved for due to the moving sulfidation surface position being unknown apriori), we employed an arbitrary-Lagrangian-Eulerian formulation as developed by Sackinger et al. (1995) and treated the mesh as a pseudo solid that obeys the following equilibrium stress equation (Sackinger et al. 1995, and Schunk et al. 1997):

$$\nabla \cdot \mathbf{T} = 0 \tag{27}$$

where

$$\mathbf{T} = 2\mu_m \mathbf{E} + \lambda_m tr(\mathbf{E})\mathbf{I} \tag{28}$$

and

$$\mathbf{E} = \frac{1}{2}\left[(\nabla \mathbf{d}) + (\nabla \mathbf{d})^T\right] \qquad (29).$$

In the above equations **d** is the mesh displacement vector, **I** is the identity matrix, and μ_m and λ_m are the Lame elastic coefficients, which are related to the familiar Young's modulus and Poisson ratio of the pseudo-solid mesh.

5.5 Position of the sulfidation surface

The position of the moving copper-sulfidation surface is determined by the local mass balance on Cu_2S being formed at the sulfidation surface (i.e., the Cu_2S/air interface):

$$\frac{dh}{dt} = \mathbf{n} \cdot (\mathbf{u}_s - \mathbf{u}_m) = \frac{M_{Cu_2S}}{\rho_{Cu_2S}} r_{Cu_2S} \qquad (30)$$

where h is the displacement or movement normal to the moving sulfidation surface relative to a mesh (which is employed in obtaining the numerical solution to Equations 10, 11 or 12, and 16) moving with local velocity $\mathbf{u}_m$, $\mathbf{u}_s$ is velocity of the sulfidation surface, and **n** is unit vector normal to the sulfidation surface; ρ_{Cu_2S} is density of Cu_2S, M_{Cu_2S} is the molecular weight of Cu_2S, and r_{Cu_2S} is the molar rate of Cu_2S formation as given by Equation 3.

5.6 Numerical solution methods, re-meshing and re-mapping

The governing equations 10, 11 or 12, and 16 are solved in GOMA, using i) finite-element discretization with structured/unstructured meshes generated by CUBIT (a Sandia-developed meshing tool, see http://endo.sandia.gov/cubit for details); ii) Galerkin weighted residuals with quadratic basis function for species concentrations, electrolyte potential, velocity, pressure, and nodal displacement unknowns; iii) a fully-coupled implicit solution scheme via Newton's method; adaptive time-step control (Adams-Bashforth predictor, Moulton corrector); and parallel computing employing an iterative solver for the solution of the resultant $\mathbf{Ax} = \mathbf{b}$ matrix-vector equations. Further details on the numerical solution method can be found in the GOMA user's guide (Schunk et al. 1997, Schunk et al. 2002). Results presented in this report were all computed on a 48-processor network of 400 MHz Sun Workstations using eight processors.

To handle the dramatic expansion in the Cu_2S domain and to avoid mesh distortion, we perform re-meshing every 10 – 20 time steps (depending on the substrate geometry, process conditions, and the state of sulfidation) using CUBIT. Solution variables were mapped from the old mesh to the new mesh using MAPVAR (a Sandia-developed utility computer program, see Wellman 1999). We automated the process of re-meshing and re-mapping using a Unix script. An example of re-meshing is presented in section 6.5.

6. Computational Results and Discussion

6.1 Verification of Goma on solving the *Poisson* equation that governs electric potential with charge separation

The one-dimensional form of Equation 16 was solved in Goma using the boundary conditions of $\Phi(0) = 0$ and $\Phi'(L) = 0$ where y is along the Cu_2S thickness direction and L is the Cu_2S layer thickness. Figure 3 compares the electric potential computed by Goma and that from the analytical solution (Equation 25) for the following parameters: L = 30 nm, $c_{V^-}(0) = 1.89\text{x}10^{-6}$ *moles/cm*^{3}, $c_{h^+}(0) = 2.04\text{x}10^{-6}$ *moles/cm*^{3}, $c_{h^+}(L) = 2.49\text{x}10^{-6}$ *moles/cm*^{3}, and $\kappa = 23.3$. As shown in Figure 3, with the Cu_2S layer being 30 nm thick and the vacancy/hole concentrations prescribed at the annihilation/sulfidation surfaces, Goma prediction agrees quite well with the analytical solution using only five uniform quadratic elements across the Cu_2S layer. As the number of elements employed in the Goma computation increases, the agreement improves as expected. With ten quadratic elements across the Cu_2S layer, electric potential predicted by Goma agrees almost perfectly well with that obtained from the analytical solution. The excellent agreement obtained here indicates that the *Poisson* equation is solved accurately in Goma. It should be pointed out that the good agreement shown in Figure 3, which was computed with relatively coarse mesh (with element size on the order of a nanometer), is attributed to two factors: 1) the concentrations of copper vacancies and electron holes are linear across the Cu_2S layer; and 2) charge separation (that is, the concentration copper vacancies differs from that of electron holes) occurs in essentially the entire Cu_2S layer. As shown later, as the copper-vacancy and electron-hole concentration profiles deviate from being linear and the charge-separation regions shrink, much smaller element size will be required in the regions with charge separation.

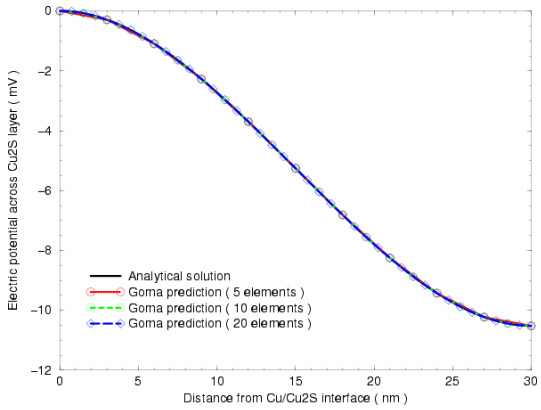

Figure 3. Comparison between analytical solution and Goma prediction – electric potential across the Cu_2S layer.

6.2 Verification of Goma for modeling transient diffusion processes involving dilute solute species and slow surface chemical reaction

A case study was carried out to systematically examine the effects of time-integration scheme and parameters on Goma predictions using a time-dependent model problem for which analytical solution can be obtained. The model problem involves a diffusion process

with a dilute solute species and a slow surface chemical reaction at one of the boundaries. Details of this case study were communicated previously (Chen 2000a) and are presented in Appendix A for convenience of reference. It was found that Goma predictions of solute-species concentration profiles agree perfectly well with that given by the analytical solution when proper time-integration scheme and parameters were employed. When inappropriate time-integration scheme or parameters were used, however, significantly incorrect results were obtained. As expected, the second-order accurate Crank-Nicholson time-integration scheme yielded more accurate predictions as compared with the first-order accurate backward-Euler method. Of the parameters used by Goma in time integration, the *maximum-time-step* parameter was found to be most effective in reducing time-integration errors. As a rule of thumb, the maximum time step allowed should be less than the time constant of the process, based on the limited findings in the case study reported here. Lastly, effect of mesh refinement was also examined and it was found that in modeling transient processes errors resulted from inappropriate use of time integration scheme and parameters are much more significant than that from the employment of an inadequately refined mesh (that is, errors from time integration are much more pronounced than that from mesh refinement).

6.3 Verification of the Goma baseline model for atmospheric copper sulfidation in the gas-phase-diffusion controlled regime with fixed sulfidation-front approximation

A case study was conducted to verify the Goma baseline model for atmospheric copper sulfidation in the gas-phase-diffusion controlled regime with the fixed sulfidation-front approximation. Details of this case study were communicated previously (Chen 2000b) and are presented in Appendix B for convenience of reference. Excellent agreement was found between Goma predictions (H_2S solute species concentration profiles and sulfide growth layer thickness) and results from the analytical solution. Effects of maximum time step allowed in Goma on H_2S solute species concentration profiles and sulfide growth layer thickness were examined and found to be significant (particularly when the maximum time steps are large) – based on the case study carried out, it was found that a maximum time step of 0.005 second yields nearly perfect agreement between Goma and analytical predictions of sulfide layer thickness. The Goma model over-predicts the sulfide layer thickness by about 3% with a maximum time step of 0.05 second, and by 18% with a maximum time step of 0.5 second. After verification, the Goma model was employed to study the effects of the boundary condition at the outer non-reacting surface on H_2S solute species concentration profiles and sulfide growth layer thickness. Lastly, to demonstrate its utility, the Goma model was exercised to compute prediction of the average sulfide layer thickness for a couple of hours of sulfidation using realistic transport/kinetic properties and process conditions, and the boundary condition of constant H_2S solute species concentration on the outer non-reacting surface.

6.4 Modeling one-dimensional copper sulfidation with charge separation

When the substrate is planar, the copper sulfidation process can be taken as one dimensional, i.e. along the thickness direction. In this section, numerical results of copper sulfidation with charge separation computed in one-dimension are presented. Here,

Equations 10, 12, and 16 were solved in one dimension (along the thickness direction) using Goma. The boundary conditions are as follow:

1) at the sulfidation surface, the normal component of the total fluxes of copper vacancies and electron holes are set to equal to the rate of sulfidation given by Equation 3 with the forward- and backward-reaction rate constants, k_1 and k_{-1} given by Equations 5 and 6, respectively.

2) at the annihilation surface, the normal component of the total fluxes of copper vacancies and electron holes are set to equal to the rate of annihilation given by Equation 4 with the rate constant, k_2, given by Equation 7.

3) at both the sulfidation and annihilation surfaces, the electric-potential gradient is zero – this is necessary in order to satisfy the zero-current (and zero-electric-field) condition there. To accomplish this within Goma, the electric potential at the annihilation surface is set to zero as a datum and the copper-vacancy concentration at the annihilation surface is iterated until the zero current constraint is met – in the present work, this was done by employing an augmenting condition in Goma.

4) Position of the moving sulfidation surface is given by Equation 30 and the internal mesh nodal displacements are computed by solving Equations 27 – 29.

Figure 4 shows a typical finite-element mesh used in a case study of simulating the one-dimensional (1-D) growth of copper sulfide. This mesh has 224 elements and results in 5,085 unknowns; it was used after the first re-meshing and re-mapping step, which is after 1.8 hours of sulfidation with a Cu_2S-layer thickness of 41.4 nm. To simulate a 1-D sulfidation process and to reduce the number of unknowns, the domain height was chosen

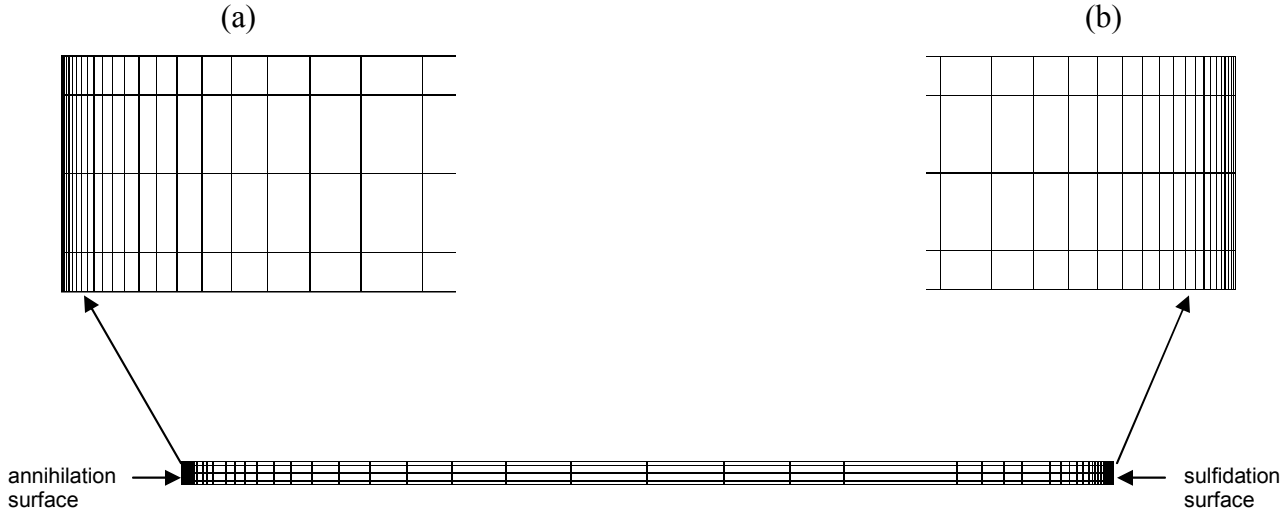

Figure 4. A typical finite-element mesh used in the 1-D simulation case study
(a) enlargement in the vicinity of the annihilation surface,
(b) enlargement in the vicinity of the sulfidation surface.

to be 3 nm and the smallest element size was fixed at 0.025 nm. As can be seen from Figure 4 and its inserts, the elements are scaled toward the annihilation and sulfidation surfaces where gradients exist. With the smallest element size being fixed at 0.025 nm, it is easy to visualize that the number of unknowns grow rapidly as the Cu_2S layer grows – this increase is due to the number of columns of elements grow in order to maintain the constant smallest element size (the number of rows of elements are held at four since the Cu_2S domain height is fixed at 3 nm).

Figure 5 displays computed concentrations of copper vacancies and electron holes across the Cu_2S layer at three different times: 1.5, 2.8, and 6.7 hours. The process parameters used in these computations came or were derived from a case study by Larson (2002): $D_{V^-} = 10^{-10}\ cm^2/s$, $D_{h^+} = 0.1\ cm^2/s$, $k_1 = 4.62\text{x}10^7\ (cm/s)(cm^3/mole)^{1/2}$, $E_1 = 6300\ cal/mole/K$, $k_{-1} = 1.2\text{x}10^{14}\ cm^{10}/mole^3/s$, $E_{-1} = 6300\ cal/mole/K$, $k_2 = 10\ cm^4/mole/s$, $E_2 = 0$, $c_{H_2S} = 400\ ppb = 1.61\text{x}10^{-11}\ moles/cm^3$, $c_{O_2} = 8.4\text{x}10^{-6}\ moles/cm^3$, $T = 303\ K$, $\kappa = 23.3$, $M_{Cu_2S} = 159.14\ g/mole$, $\rho_{Cu_2S} = 5.6\ g/mole$. In addition, the two Lame elastic coefficients used are: $\mu_m = 1$, $\lambda_m = 1$. As can be seen from Figure 5, thickness of the space-charge layers (in which charge separation occurs, that is, concentration of copper vacancies differs from that of electron holes) decreases as the Cu_2S layer grows thicker. More specifically, as indicated in the caption of Figure 5, at t = 1.5 hours, the Cu_2S layer thickness (h) is 30 nm whereas the space-charge layer thickness (h_{sc}) is 13.3 nm such that h_{sc}/h = 44.3% (that is, charge separation occurs in 44.3% of the Cu_2S layer). As time increases to 2.8 hours, h_{sc}/h decreases to 13.1%. By the time of 6.7 hours, h_{sc}/h has dropped to 4.3%. Figure 6 further shows how the space-charge layer shrinks as the Cu_2S layer grows thicker. Here, the space-charge layer thickness was so computed that $|(c_{V^-} - c_{h^+})/c_{V^-}| > 0.01$ within the space-charge layers (that is, concentration of copper vacancies differs from that of electron holes by more than 1%). As can be seen clearly from Figure 6, thickness of the space-charge layers decreases rapidly as the Cu_2S layer thickens initially, but it tends to level off as Cu_2S layer becomes sufficiently thick, and eventually reaches a steady-state or equilibrium value around 2 nm.

Figure 7 shows the computed electric potential across the sulfide layer at various times. To help examine the gradients at the annihilation and sulfidation surfaces, Figure 8 displays the electric potential at 1.8 hours whereas Figure 9 shows the electric potential at 80 hours with the inserts providing the enlarged views near the annihilation and sulfidation surfaces, respectively. As can be discerned from Figures 8 and 9, the zero-current (and zero-electric-field) boundary condition is met at both the annihilation and sulfidation surfaces since the slopes there essentially vanish (i.e., are essentially zero). As is shown in Figure 7, away from the space-charge layers, the electric-potential gradient decreases with time and from the annihilation to sulfidation surface. Figure 10 further shows how the electric potential at the sulfidation surface decreases with the Cu_2S layer thickness; clearly, the electric potential at the sulfidation surface decreases rapidly as the Cu_2S layer thickens initially, but it then levels off as the Cu_2S layer becomes sufficiently thick (e.g., about 500 nm) and eventually reaches a steady-state or equilibrium value around -39 mV. It may be speculated that the value of -39 mV is due to the difference in diffusion coefficients between D_{h^+} and D_{V^-}. More studies are needed to determine if this is indeed the case. When the Cu_2S layer grows to be 1 μm thick, the electric potential at the sulfidation surface is about -37 mV, relative to the zero datum electric potential at the annihilation surface. To check if Equation 18 provides a reasonable approximation for computing the electric-potential gradient, which is needed in order to account for the migration flux (as described in Equation 12), we solved Equations 10, 11, 25 – 28 and computed $\nabla\Phi$ using Equation 18.

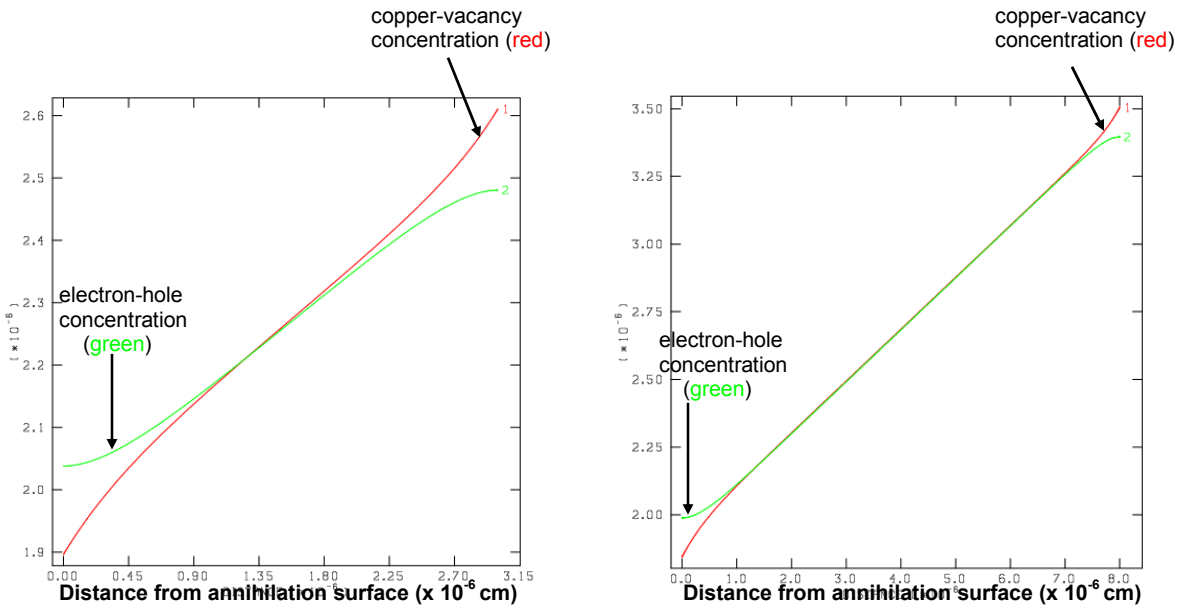

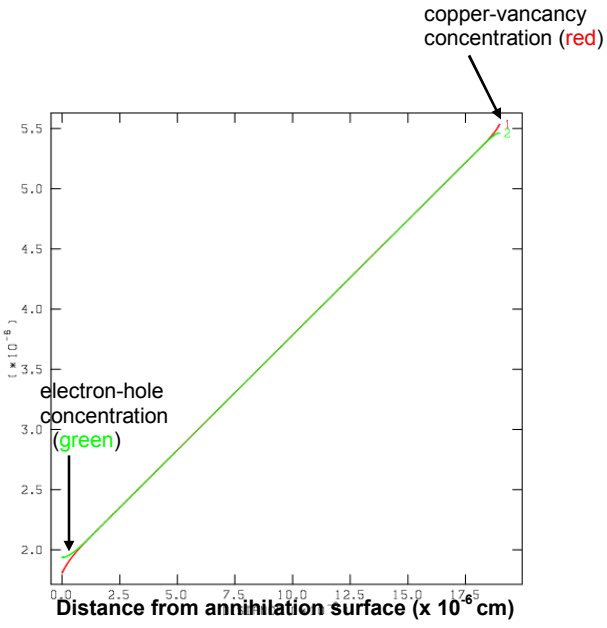

(c)

Figure 5. Computed concentrations of copper vacancies and electron holes across Cu_2S layer at various times.

(a) t = 1.5 hours, h = 30 nm, h_{sc} = 13.3 nm, h_{sc}/h = 44.3%;
(b) t = 2.8 hours, h = 80 nm, h_{sc} = 10.5 nm, h_{sc}/h = 13.1%;
(c) t = 6.7 hours, h = 190 nm, h_{sc} = 8.1 nm, h_{sc}/h = 4.3%.
(h_{sc} is thickness of the space-charge layer with charge separation)

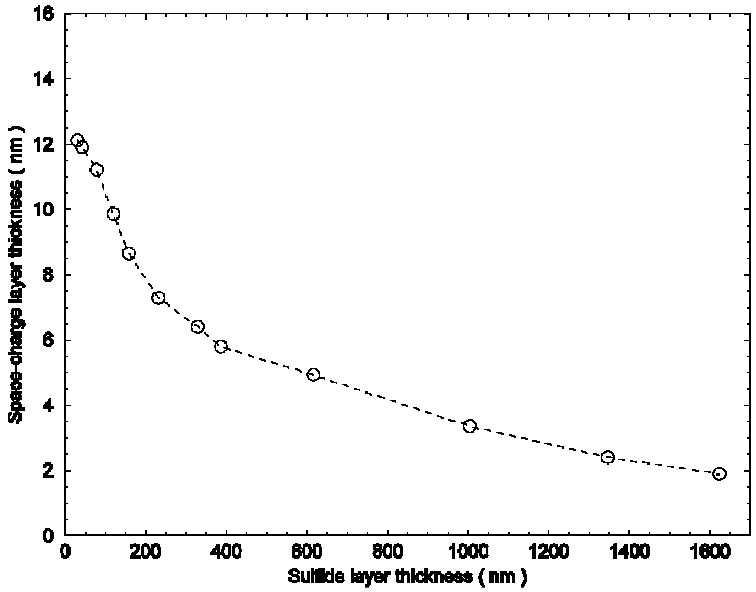

Figure 6. Computed space-charge layer thickness as a function of Cu_2S layer thickness

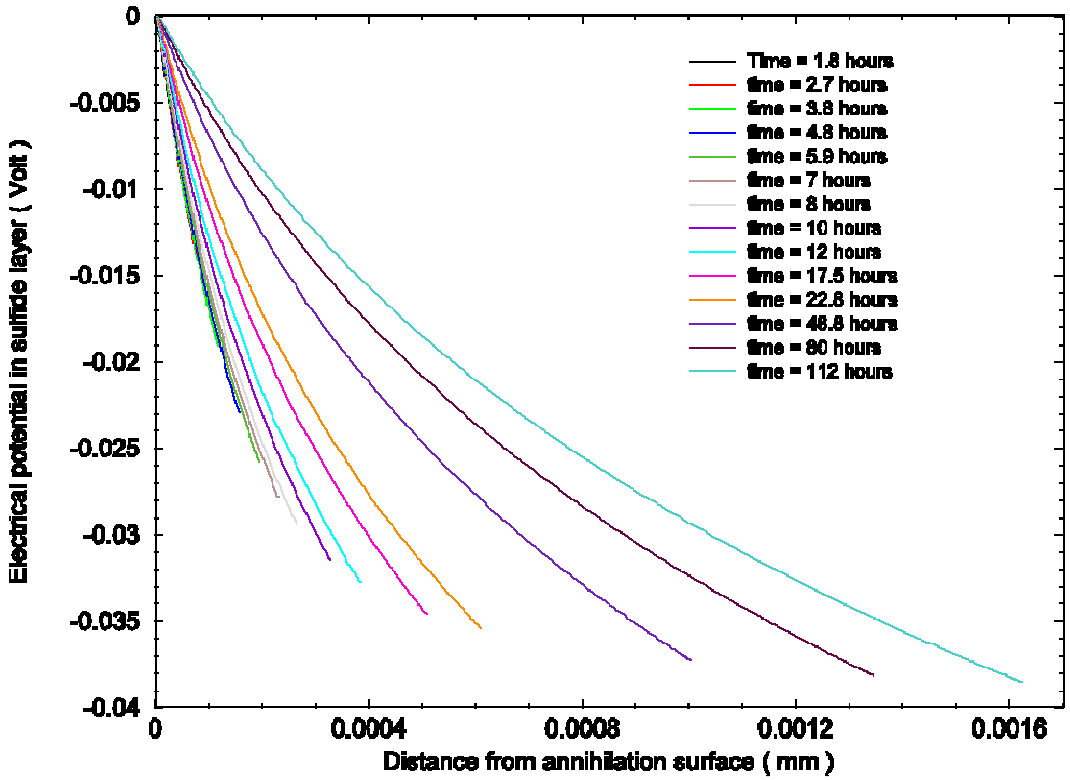

Figure 7. Computed electric potential across the Cu_2S layer at various times

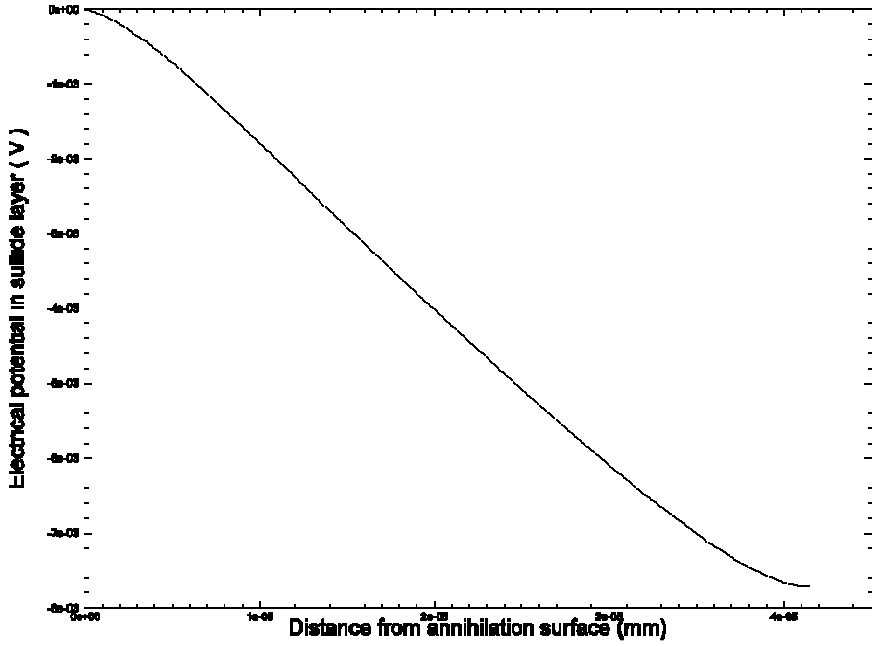

Figure 8. Computed electric potential across the Cu_2S layer at t = 1.8 hours

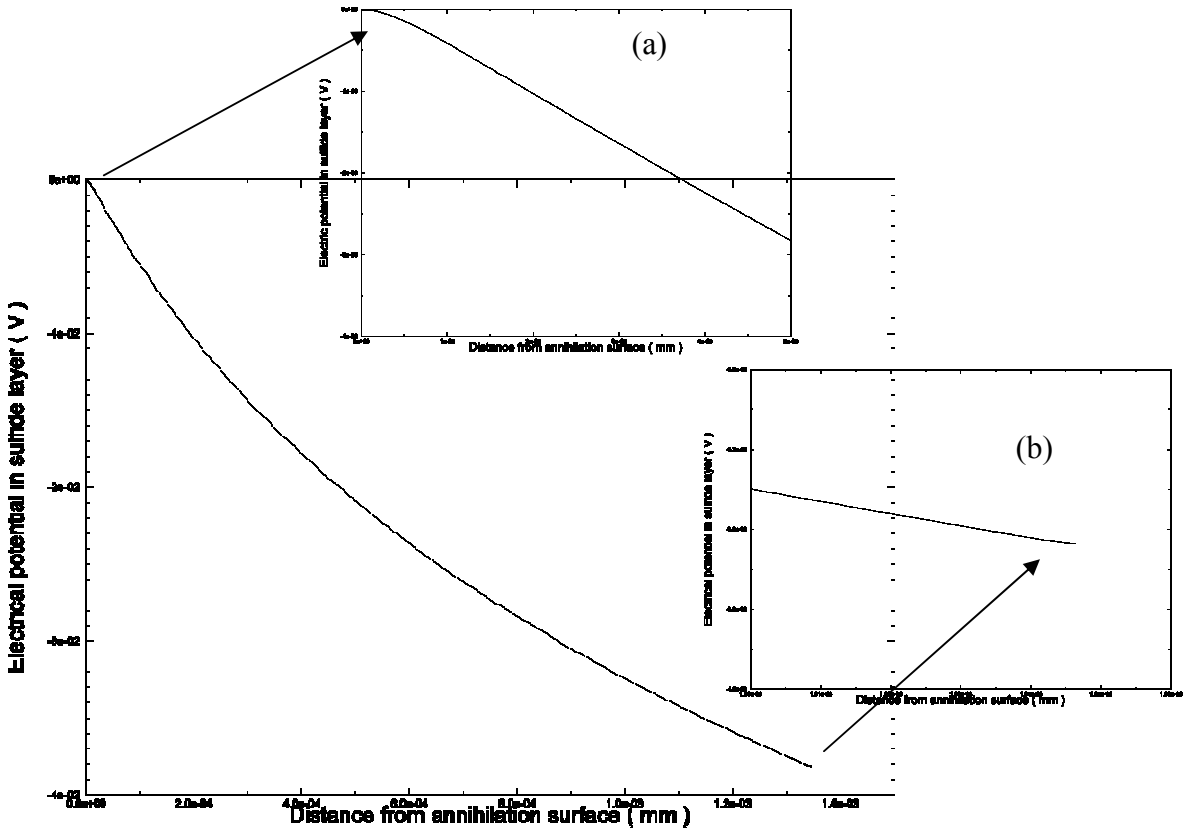

Figure 9. Computed electric potential across the Cu_2S layer at t = 80 hours
(a) enlargement near annihilation surface;
(b) enlargement near sulfidation surface.

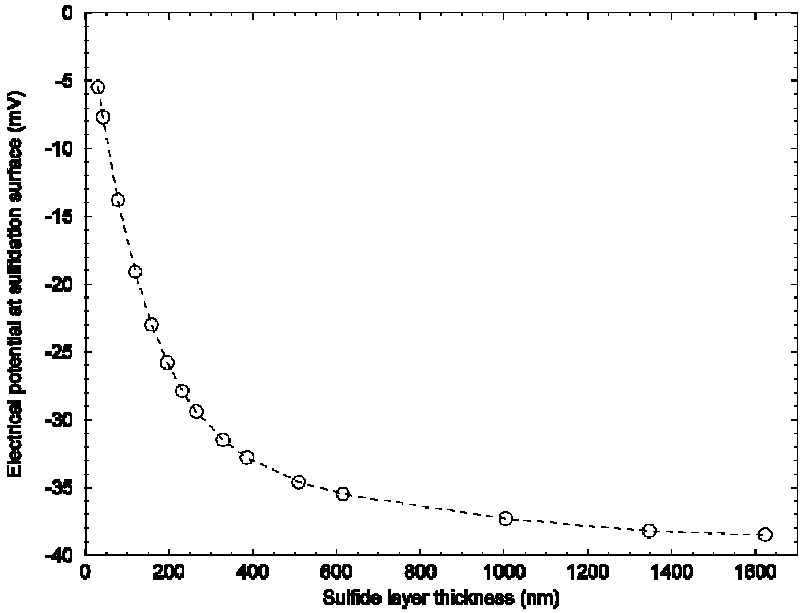

Figure 10. Computed electric potential at the sulfidation surface as a function of Cu_2S layer thickness

The computed Cu_2S layer thickness as a function of time is plotted in Figure 11 along with experimental data obtained by Rob Sorensen and Jeff Braithwaite and presented by Larson (2002). The good agreements between the computed model predictions and experimental data for three different concentrations of H_2S appear to indicate that electroneutrality is a reasonable approximation and that Equation 18 can be used to estimate the electric-potential gradient when the Cu_2S layer grows to be sufficiently thick. Larson (2002) has also found that "an assumption of electroneutrality in the sulfide, which can drastically simplify the computations, give rise to very little error under typical conditions". In any case, further research efforts are needed in order to determine the difference of electric potentials between the annihilation and sulfidation surfaces so that the electric-potential gradient can be estimated from Equation 18 to avoid performing the computationally costly operation, namely solving the Poisson equation (Equation 16) with the stringent zero-current (and zero-electric-field) boundary conditions at the annihilation and sulfidation surfaces.

6.5 Modeling copper sulfidation on a prototypical diode

Figure 12 shows an image of sulfidation on a copper-containing braze in a zener diode, which was obtained in a field test by Roben Sorensen and Jeff Braithwaite (Braithwaite et al. 2003). Figure 13 displays a model geometry of copper sulfidation on a prototypical diode, which is consisted of a silicon device connected to two copper cylinders that are connected to two silver-plated copper leads. It should be noted that the model geometry (as depicted in Figure 13) for sulfidation on diode surface has been greatly simplified since

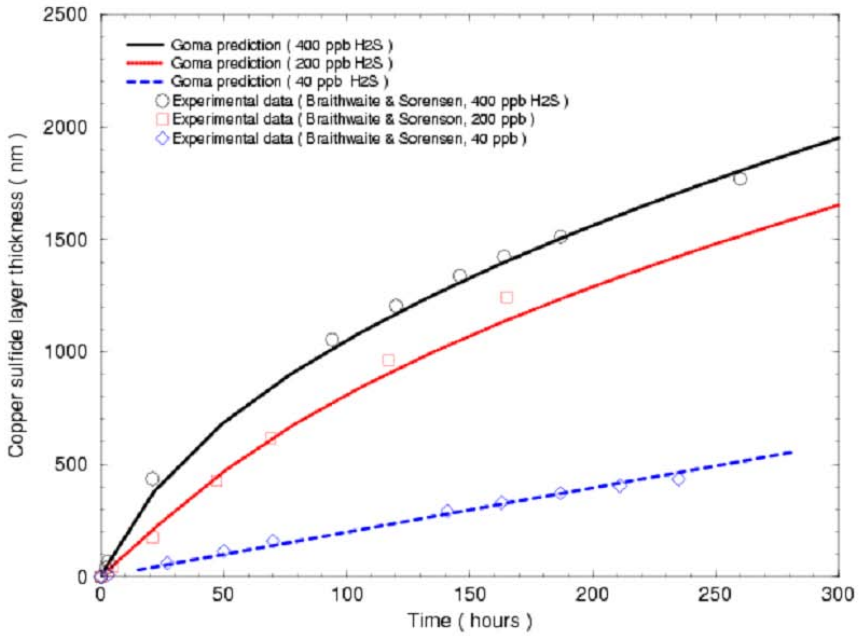

Figure 11. Cu_2S layer thickness as a function of time
(Model parameters are the same as those for Figures 4 – 7;
electric potential at sulfidation surface fixed at -37 μV,
electric potential at annihilation surface set to 0 as datum).

in practice diodes are normally encapsulated by porous epoxy resin. In the present study, the resistance to copper-vacancy transport in the silver plating is considered so high that annihilation of copper vacancies and electron holes take place only at the Cu/Cu_2S interface; that is, the two copper cylinders serve as sources for Cu and sinks for V^- and h^+. An example of re-meshing is presented in Figure 14. Here, only a quarter of the cylindrical substrate surfaces and Cu_2S phase or domain are displayed. The total number of unknowns for the starting mesh is around 30,000. As can be seen from Figure 14, as sulfidation proceeds, the Cu_2S domain expands and its shape changes drastically – at each re-meshing step the mesh topology was modified accordingly by employing CUBIT and the nodal unknowns were mapped from the old mesh to the new mesh by using MAPVAR. In this example, it took more than ten re-meshing operations to simulate the sulfidation process until a continuous Cu_2S phase is formed on the diode surface. To keep the computation manageable, the minimum element size was increased accordingly at each re-meshing step. This seems reasonable when the Cu_2S layer is sufficiently thick so that charge separation in the space-charge layers can be neglected and the entire Cu_2S domain can be taken to be electro-neutral (that is, it is not necessary to solve Equation 16 with the zero-current boundary conditions at the annihilation and sulfidation surfaces).

Figure 15 shows a case-study of Goma simulation of copper sulfidation on a prototypical diode in the solid-state-diffusion controlled regime (that is, Stage II sulfidation in which the copper-vacancy and electron-hole transport is limiting; the concentration of H_2S at the sulfidation surface is taken to be constant). The process parameters used in the case study are:

Figure 12. Sulfidation of a copper-containing braze in a zener diode (Braithwaite et al. 2003)

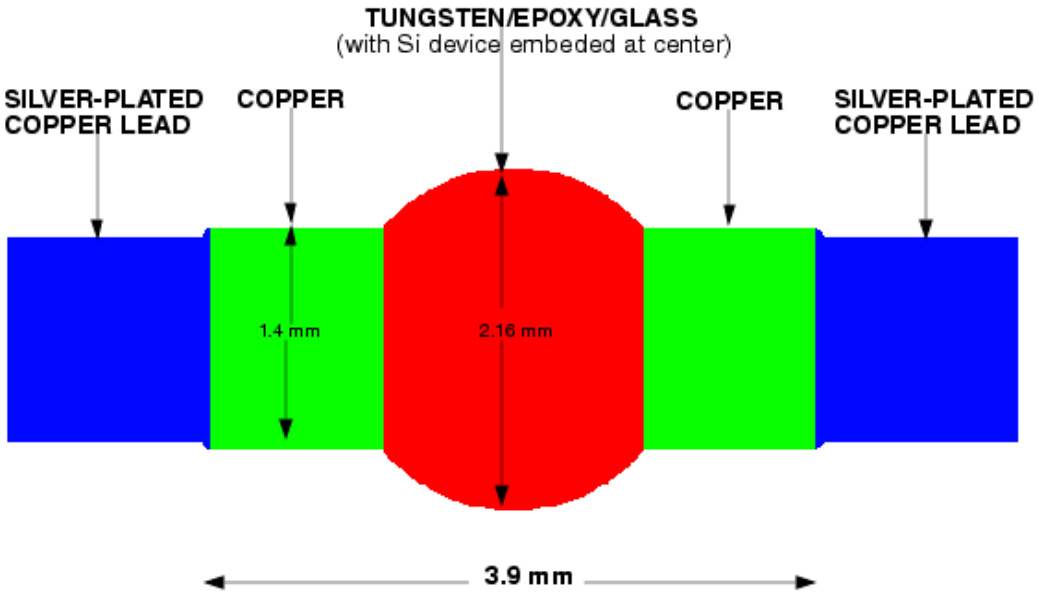

Figure 13. Model geometry of copper sulfidation on a prototypical diode

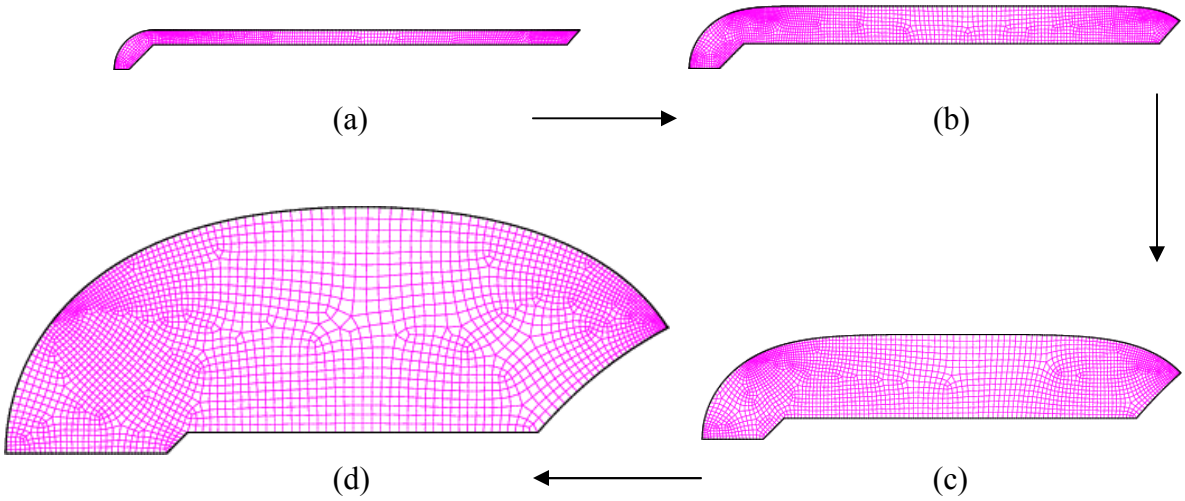

Figure 14. An example of re-meshing in modeling copper sulfidation on a diode (only a quarter of the substrate surface and Cu_2S domain are displayed) (a) starting mesh; (b) second re-meshing; (c) fourth re-meshing; (d) nineth re-meshing.

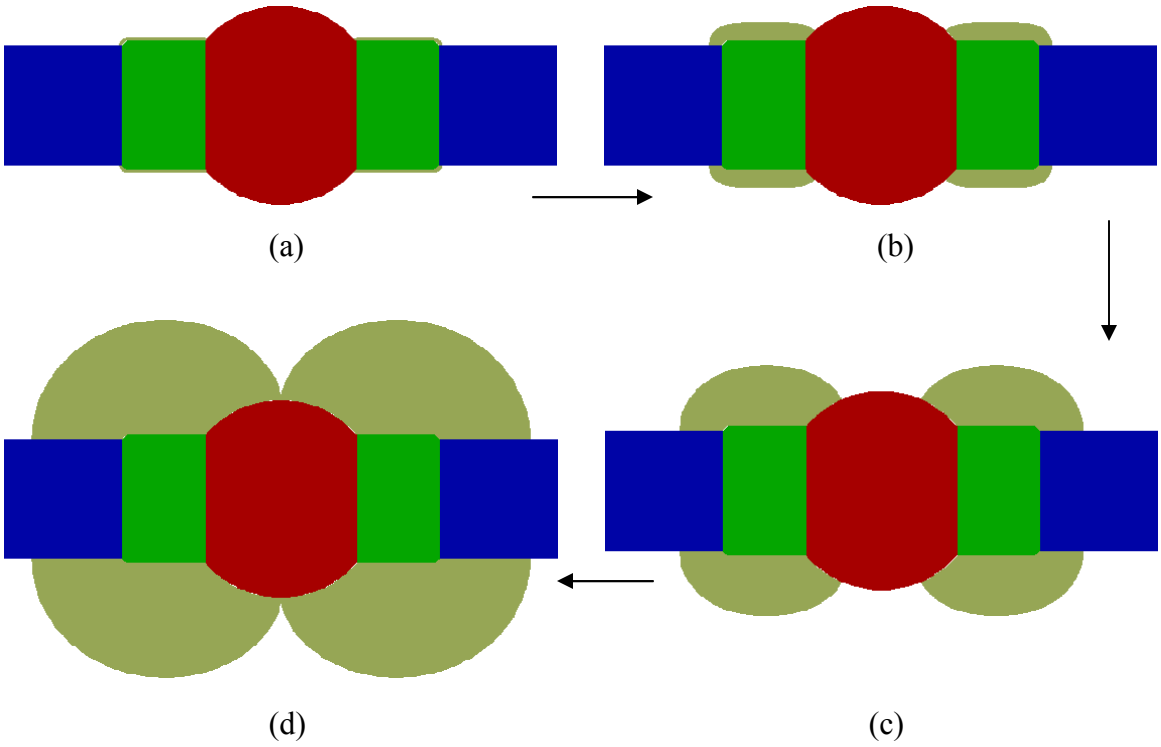

Figure 15. Sample Goma predictions of copper sulfidation on a prototypical diode in the solid-state-diffusion controlled regime (i.e. stage II sulfidation). (a) time ~ 1 year; (b) time ~ 100 years; (c) time ~ 1500 years; (d) time ~ 7000 years.

$D_{V^-} = 10^{-10}\, cm^2/s$, k_1 = 1.46x10^7 $(cm/s)(cm^3/mole)^{1/2}$, E_1 = 6300 *cal/mole/K*, k_{-1} = 1.2x10^{14} $cm^{10}/mole^3/s$, E_{-1} = 6300 *cal/mole/K*, k_2 = 10 $cm^4/mole/s$, E_2 = 0, $c_{H_2S} = 400$ *ppm* = 1.61x10^{-8} *moles/cm*^{3}, $c_{O_2} = 8.4\text{x}10^{-6}$ *moles/cm*^{3}, T = 303 *K*, $M_{Cu_2S} = 159.14$ *g/mole*, $\rho_{Cu_2S} = 5.6$ *g/mole*, μ_m = 1, λ_m = 1, $\theta_{c,Cu_2S/Si}$ = 60^o ($\theta_{c,Cu_2S/Si}$ is angle of contact between Cu_2S and silicon-device surface), $\theta_{c,Cu_2S/Ag}$ = 90^o ($\theta_{c,Cu_2S/Ag}$ is angle of contact between Cu_2S and silver-plating surface). In this case study, the Cu_2S domain was taken to be electro-neutral, that is, $c_{V^-} = c_{h^+}$, and the migration flux was neglected. With the diode geometry as specified in Figure 13 and process parameters chosen as above, it takes ~ 7000 years for a continuous Cu_2S film to form on the diode surface as shown in Figure 15d. The effect of bulk H_2S concentration on time required to form a continuous Cu_2S film on diode surface in the solid-state-diffusion regime is displayed in Figure 16. The process parameters are the same as presented above except here c_{H_2S} was varied from 400 ppb to 400 ppm. As expected, time required to form a continuous Cu_2S film on diode surface increases rapidly as corrodant H_2S concentration is lowered.

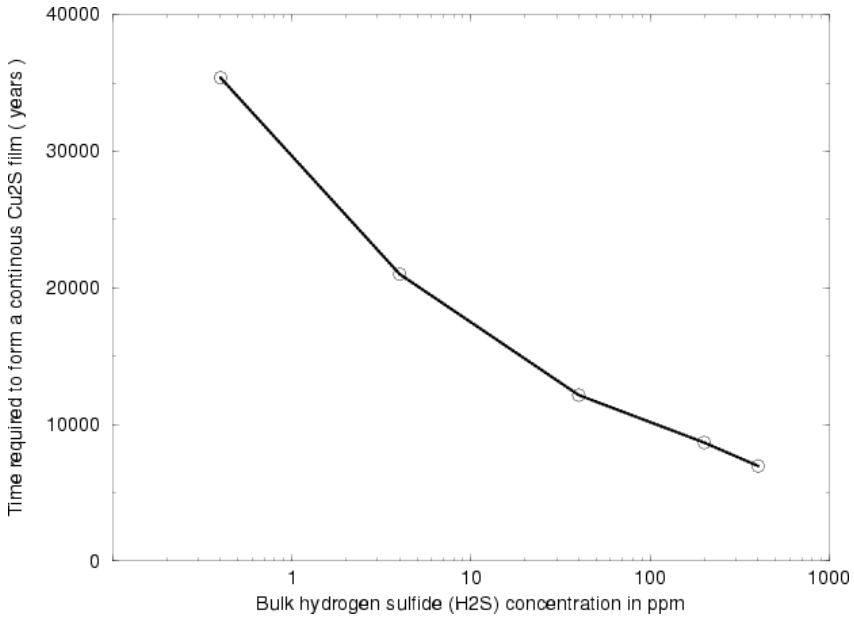

Figure 16. Effect of bulk H_2S concentration on time required to form a continuous Cu_2S film on the diode surface.

Lastly, Figure 17 displays a case-study of Goma simulation of copper sulfidation on a prototypical diode in the gas-phase-diffusion controlled regime. In other words, Stage I sulfidation in which the H_2S diffusion in the surrounding gas and the sulfidation electrochemical reaction are limiting as compared with solid-state transport. The rate of sulfidation depends on H_2S concentration at the sulfidation surface only. Strictly speaking, gas-phase diffusion is limiting only in the early stage of the sulfidation process and solid-state diffusion is mostly limiting. Nevertheless, results from this case study are presented in

Figure 17 to demonstrate the utility of the Goma framework for modeling atmospheric copper sulfidation, which involves corrodant H_2S diffusion in the surrounding gas. Here, the rate of copper sulfidation is taken to depend on H_2S concentration at the sulfidation surface only, i.e. $r_{Cu_2S} = K_1 c_{H_2S}$, and the process parameters are: $c_{H_2S,bulk} = c_{H_2S,initial} = 400$ *ppb* = 1.61x10^{-11} *moles*/*cm*^{3}, $K_1 = 2$ cm/s, $D_{H_2S} = 0.1$ cm^2/s, $\mu_m = 1$, $\lambda_m = 1$, $\theta_{c,Cu_2S/Si} = 30^o$. As can be seen in Figure 17, the time required to form a continuous Cu_2S film on the diode surface would be considerably shorter if the sulfidation process was gas-phase-diffusion controlled.

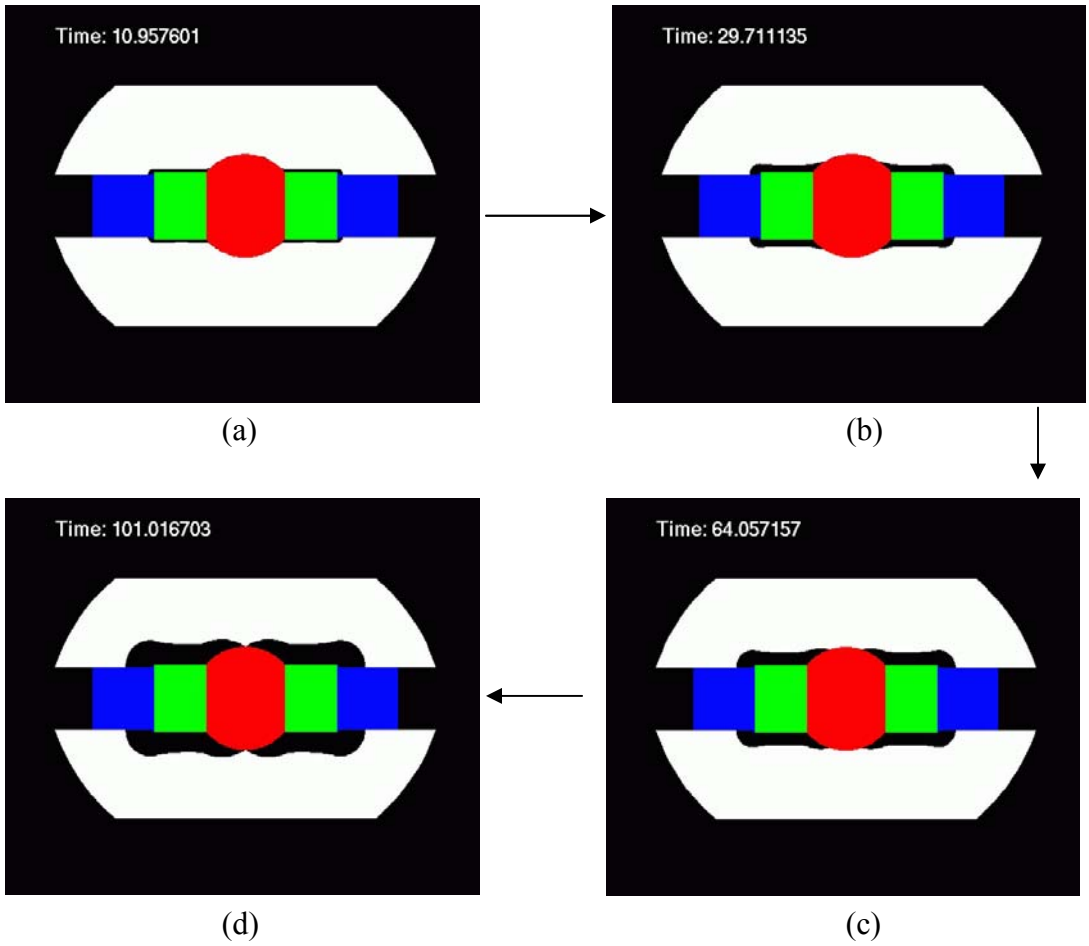

Figure 17. Sample Goma predictions of copper sulfidation on a prototypical diode in the gas-phase-diffusion controlled regime (i.e. Stage I sulfidation). (a) time ~ 11 years; (b) time ~ 30 years; (c) time ~ 64 years; (d) time ~ 101 years.

Color indicators:
green – copper portion of diode, blue – silver-plated copper lead;
red – tungsten/epoxy/glass silicon device, white – gas phase region;
black (between diode and gas phase) – copper sulfide.

6.6 Modeling copper sulfidation on an intermittent electrical contact

Figure 18 shows a schematic of copper-sulfidation corrosion on an electrical contact. Here, a gold-plated copper pin (at top) is supposed to make good contact intermittently with a gold-plated copper contact pad (at bottom). Now, suppose that a pinhole is present in the gold plating (pinholes are present due to the imperfect plating process or impurity on substrate surface) such that the copper pad is exposed to the surrounding gas polluted with corrodant H_2S for an extended time period in a relatively high-humidity, sulfidizing environment. Consequently, copper sulfide will grow inside the pinhole and then outside it. Figure 19 shows the simulated stage II copper sulfidation inside a pinhole with a diameter

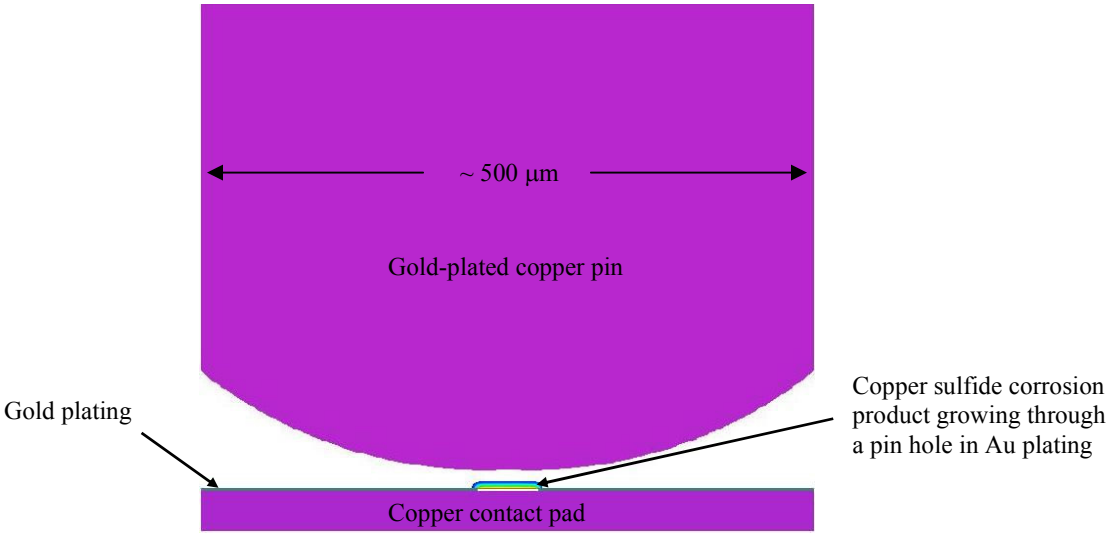

Figure 18. Schematic of copper-sulfidation corrosion on electrical contact

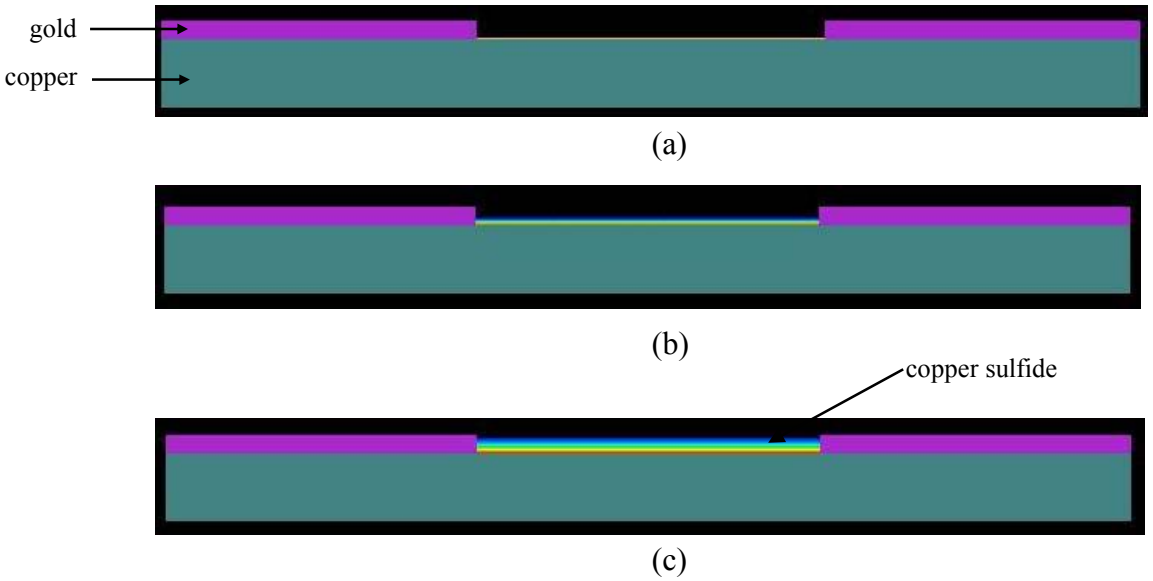

Figure 19. Simulated growth of copper sulfide inside a pinhole
(a) time ~ 1 hour; (b) time ~ 2 days; (c) time ~ 10 days.

of 25 μm and a height of 1.5 μm. The process parameters used in this case study are: $D_{V^-} = 10^{-10}\ cm^2/s$, $k_1 = 4.62\text{x}10^7\ (cm/s)(cm^3/mole)^{1/2}$, $E_1 = 6300\ cal/mole/K$, $k_{-1} = 1.2\text{x}10^{14}\ cm^{10}/mole^3/s$, $E_{-1} = 6300\ cal/mole/K$, $k_2 = 10\ cm^4/mole/s$, $E_2 = 0$, $c_{H_2S} = 400\ ppb = 1.61\text{x}10^{-11}\ moles/cm^3$, $c_{O_2} = 8.4\text{x}10^{-6}\ moles/cm^3$, $T = 303\ K$, $M_{Cu_2S} = 159.14\ g/mole$, $\rho_{Cu_2S} = 5.6\ g/mole$, $\mu_m = 1$, $\lambda_m = 1$, $\theta_{c,Cu_2S/Au} = 90^o$ ($\theta_{c,Cu_2S/Au}$ is the angle of contact between Cu_2S and gold plating). In this case study, the migration flux has been neglected. With the parameters specified and as can be seen from Figure 19, it takes about 10 days to fill the 1.5μm-deep pinhole with Cu_2S. Figure 20 displays the simulated growth of stage II copper sulfidation outside the pinhole (process parameters are the same as described above for sulfidation inside the pinhole). As sulfidation proceeds, the Cu_2S corrosion product tends to form a hemisphere – this is expected since a hemisphere will yield equal diffusional distance for V^- and h^+ from the center of the pinhole to the sulfidation surface with the pinhole serving as a point source for Cu (and sink for V^- and h^+) when the Cu_2S domain becomes sufficiently large.

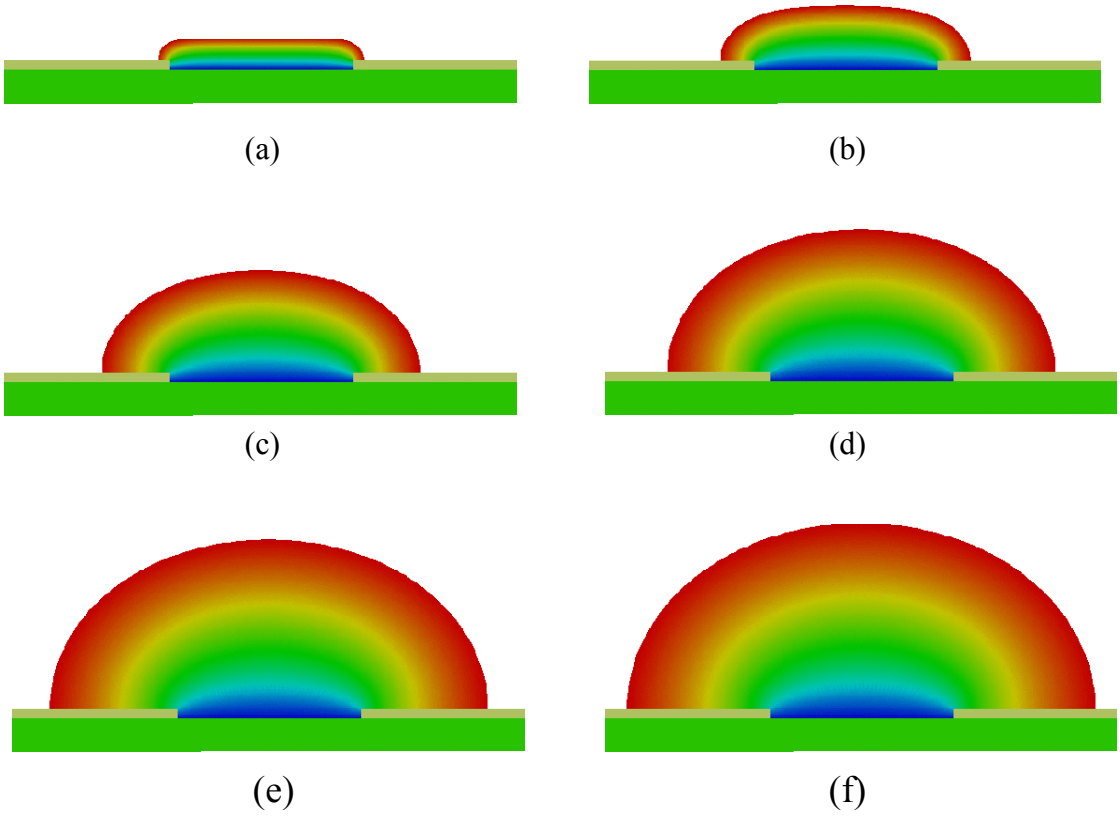

Figure 20. Simulated growth of copper sulfide outside a pinhole
(a) time ~ 0.1 year; (b) time ~ 1.2 year; (c) time ~ 5 years;
(d) time ~ 10 years; (e) time ~ 15 years; (f) time ~ 18 years.

As soon as the growing domain of the Cu_2S corrosion product is determined as shown in Figures 19 & 20, the electrical potential field within the pin-Cu_2S-pad electrical contact assembly (Figure 21) can be computed by solving Equation 16 with the right-hand side set to zero (that is, electroneutrality is valid everywhere within the electrical contact assembly) and $\kappa\varepsilon_0$ set to be the electrical conductivity of the respective materials in the assembly. Once the electrical potential within the pin-Cu_2S-pad electrical contact assembly is known, the total electrical current being conducted through the assembly, I, can be readily computed from:

$$I = \int (-\kappa' \nabla \Phi) dA \tag{31}$$

where κ' is the local electrical conductivity of the material in which I is computed, and Φ is the electrical potential in the pin-Cu_2S-pad electrical contact assembly and A is the cross-sectional area. Finally, the effective electrical resistance of the assembly, R, is numerically computed within Goma by using Ohm's law:

$$R = \frac{\Delta\Phi}{I} = \frac{1}{\int (-\kappa' \nabla \Phi) dA} \tag{32}$$

where $\Delta\Phi$ is the electrical potential difference between the surface of the copper pad and the top surface of the copper pin and can be conveniently chosen to be unity (i.e. 1 volt); the electrical potential at the copper-pad and top copper-pin surfaces are accordingly set to 0 and 1 volt, respectively, as the boundary conditions for solving Equation 16 with the right-hand side set to zero. Figure 21a shows a typical finite element mesh used in computing the electrical potential in the pin-Cu_2S-pad electrical contact assembly whereas Figure 21b displays the electrical potential contours after about 50 years of sulfidation. In this case study, an electrical conductivity of 37 $\Omega^{-1}cm^{-1}$ for Cu_2S was used, which is within the range (15 to 52 $\Omega^{-1}cm^{-1}$) of conductivity at room temperature as reported by Okamoto and Kawai (1973) for Cu_2S grown from a stoichiometric mixture. The presence of Cu_2S results in an increase of effective electrical resistance for the pin-Cu_2S-pad electrical contact assembly by a factor around 5000 as compared with case when Cu_2S is absent. This was determined by computing the effective resistances for the contact assembly with and without the corrosion product and then taking the ratio of the two effective resistances. Note that the large rectangular structure at the top of Figure 21b represents the electrical contact pin and the Cu_2S corrosion product is the banded structure near the bottom. As shown, this Cu_2S mound was taken to be deformable and the contact interface conforms to the rigid flat surface of the gold-plated copper pin.

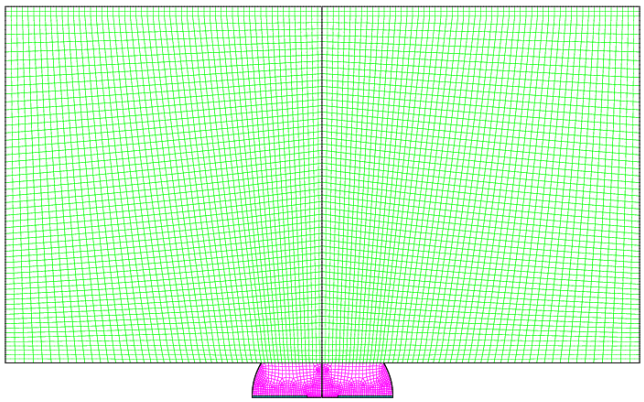

(a)

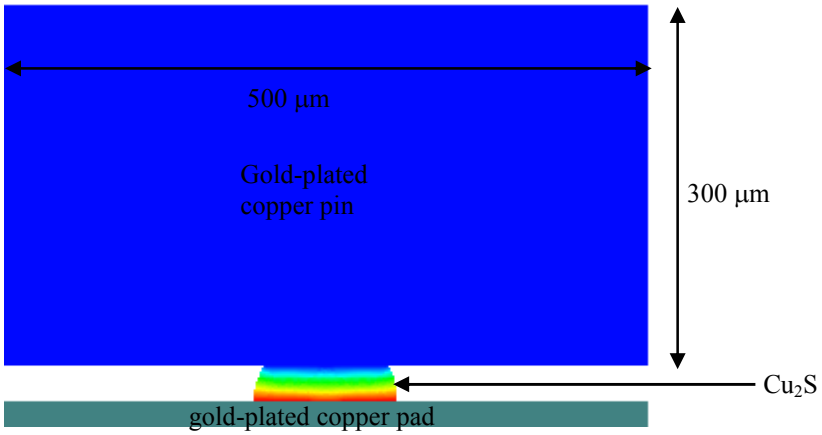

(b)

Figure 21. Pin-Cu_2S-pad electrical contact assembly
(a) finite element mesh;
(b) electrical potential contours at t ~ 50 years.

7. Summary and Concluding Remarks

A new framework based on Goma was developed and demonstrated for multi-dimensional modeling of atmospheric copper-sulfidation corrosion on non-planar substrates such as diodes and electrical contacts. In this framework, the moving sulfidation front is explicitly tracked by treating the finite-element mesh as a pseudo solid with an arbitrary Lagrangian-Eulerian formulation and repeatedly performing re-meshing using CUBIT and re-mapping using MAPVAR. To gain confidence on the framework, three one-dimensional Goma-verification studies were carried out: 1) on solving the *Poisson* equation that governs electrical potential with charge separation in an asymptotic regime in which the copper-vacancy and electron-hole concentrations can be approximated as linear across the Cu_2S; 2) for modeling transient diffusion processes involving dilute solute species and slow surface chemical reaction; and 3) for modeling atmospheric copper sulfidation in the gas-phase-diffusion controlled regime with fixed sulfidation-front approximation.

The framework was first demonstrated in modeling one-dimensional copper sulfidation with charge separation. It was found that both thickness of the space-charge layers and electrical potential at the sulfidation surface decrease rapidly as the Cu_2S layer thickens initially, but they tend to level off as Cu_2S layer becomes sufficiently thick, and eventually reach steady-state values. Moreover, computed results from a case study indicate that electroneutrality is a reasonable approximation and that the electro-migration flux can be estimated by using a constant potential difference (-37 mV) between the sulfidation and annihilation surfaces when the Cu_2S layer grows to be sufficiently thick. It has also been reported by Larson (2002) that "an assumption of electroneutrality in the sulfide, which can drastically simplify the computations, give rise to very little error under typical conditions". Being able to employ the electroneutrality approximation is very helpful since the computationally costly operation of solving the Poisson equation with the stringent zero-current boundary conditions at the annihilation and sulfidation surfaces can be avoided. The framework was then employed to model copper sulfidation on a prototypical diode until a continuous Cu_2S film was formed on the diode surface. As expected, the time required to form a continuous Cu_2S film on the diode surface increases rapidly as the corrodant H_2S concentration was lowered. Lastly, the framework was applied to model copper sulfidation on an intermittent electrical contact between a gold-plated copper pin and gold-plated copper pad; the presence of Cu_2S was found to raise the effective electrical resistance drastically.

Though significant progress has been made in the deterministic modeling of the complex atmospheric copper-sulfidation process, research efforts are needed in several areas: 1) develop constitutive models to account for the effects of humidity (available but conflicting experimental observations have made this task difficult) and liquid water (droplets or continuous layer); 2) incorporate effect of Kirkendall voiding at the Cu/Cu_2S interface (which is due to localized depletion of copper metal); 3) capture the effects of Cu_2S microstructure (defect structure and density) on copper-vacancy transport; 4) measure or compute the thermodynamic equilibrium constants and relate these equilibrium constants to the free energy of formation of the vacancies and holes in Cu_2S; and 5) perform additional model validation; only very limited model validation was carried out but much more are needed.

8. References

Barbour, J. C., Sullivan, . P., Campin, M. J., Wright, A. F., Missert, N. A., Braithwaite, J. W., Zavadil, Sorensen, N. R., Lucero, S. J., Breiland, W. G., and Moffat, H. K., "Mechanisms of atmospheric copper sulfidation and evaluation of parallel experimentation techniques", *SAND Report SAND2002-0699* (2002).

Braithwaite, J., Larson, R. S., Moffat, H. K., Breiland, W. G., Sorensen, N. R., and Barbour, J. C., "The effect of gas-phase mass transport on the atmospheric sulfidation of copper", paper presented at the *Fall 2000 Electrochemical Society Meeting – Electrochemical Science and Technology of Copper Symposium*, Phoenix, AZ, October 22 – 27, 2000.

Braithwaite, J., "Copper sulfidation – constitutive equations", Sandia internal email, April 17, 2002.

Braithwaite, J., Sorensen, N. R., Robinson, D., Chen, K. S., and Bogdan, C., "A modeling approach for predicting the effects of corrosion on electrical-circuit reliability", *SAND Report* SAND2003-0359 (2003).

Campin, M. J., *Microstructural Investigation of Copper Corrosion: Influence of Humidity*, Ph.D. Thesis, New Mexico State University (2003).

Chen, K. S., "A baseline multi-dimensional mathematical model of copper sulfidation for the initial implementation in Goma, *Sandia technical memorandum* issued on January 22, 1999.

Chen, K. S., "On the verification of Goma's capability for modeling transient diffusion processes involving dilute solute species and slow surface chemical reaction", *Sandia technical memorandum* issued on March 31, 2000.

Chen, K. S., "On the verification of Goma baseline model for atmospheric copper sulfidation in the gas-phase diffusion regime – fixed sulfidation-front approximation", *Sandia technical memorandum* issued on May 5, 2000.

Chen, K. S., "Progress report on continuum modeling of copper sulfidation corrosion: incorporation of an improved sulfidation model in Goma and comparison with Larson's numerical-model prediction and with Braithwaite & Sorensen's experimental data", presentation at the Corrosion Initiative Working Group, April 9, 2002.

Chen, K. S., "On implementing and verifying in Goma the Poisson equation governing electric potential in electrochemical processes involving charge separation such as in copper sulfidation", *Sandia technical memorandum* issued on May 15, 2002.

Chen, K. S., "Goma modeling of atmospheric copper sulfidation with charge separation", *Sandia technical memorandum* issued on June 30, 2003.

Chen, K. S., "Continuum modeling of atmospheric copper-sulfidation corrosion on non-Planar substrates", paper presented at the *5th Biennial Tri-Laboratory Engineering Conference on Modeling and Simulation*, Santa Fe, NM, October 21 – 23, 2003.

Enos, D. G., Dalton, S. D., and Braithwaite, J. W., "An investigation of how humidity can affect atmospheric copper sulfidation kinetics", a paper presented at the *202nd Meeting of the Electrochemical Society*, Salt Lake City, UT, October 20 – 25, 2002.

Enos, D. G., Glauner, C. S., and Sorensen, N. R., "The atmospheric degradation of gold and nickel-gold electroplated copper connectors", a paper presented at the *Electrochemical Society Fall 2003 Annual Meeting*, Orlando, FL, October 13 – 17, 2003.

Graedel, T. E., Franey, J. P., and Kammlott, G. W., "The corrosion of copper by atmospheric sulphurous gases", *Corrosion Science*, Vol. 23, pp. 1141 – 1152 (1983).

Graedel, T. E., Franey, J. P., Gualtieri, G. J., Kammlott, G. W., and Malm, D. L., "On the mechanism of silver and copper sulfidation by atmospheric H_2S and OCS", *Corrosion Science*, Vol. 25, pp. 1163 – 1180 (1985).

Graedel, T. E., Franey, J. P., Kammlott, G. W., and Vandenberg, J. M., "The atmospheric sulfidation of copper single crystals", *J. Electrochem. Soc.*, Vol. 134, pp. 1633 (1987).

Graedel, T. E., "GILDES model studies of aqueous chemistry. I. formulation and potential applications of the multi-regime model", *Corrosion Science*, Vol. 38, pp. 2153 (1996).

Krska, C., Stimetz, C., Braithwaite, J., Sorensen, R., and Hlava, P., "Corrosion of SA1388-1 diodes", paper presented at the *20th Compatibility, Aging and Stockpile Stewardship Conference*, Kansas City, KS, April 30 – May 2, 1996.

Larson, R. S., "A physical and mathematical model for the atmospheric sulfidation of copper by hydrogen sulfide", *Sandia Report*, SAND98-8613 (1998).

Larson, R. S., "A physical and mathematical model for the atmospheric sulfidation of copper by hydrogen sulfide", *J. Electrochem. Soc.*, Vol. 149, pp. B40-B46 (2002).

Leygraf, C. and Graedel, T. E., Atmospheric Corrosion, Wiley-Interscience, New York (2000).

Moffat, H., Nelson, J., Barbour, J. C., Braithwaite, J. W., Breiland, W. G., Chen, K. S., Cygan, R. T., Larson, R. S., and Teter, D. M., "Multi-length scale modeling of atmospheric sulfidation of copper", paper presented at the *2000 Spring MRS Meeting*, San Francisco, CA, April 24 – 28, 2000.

Moffat, H., "Analysis of a stagnation point flow reactor design for use in corrosion experiments – Braithwaite's effluent experiments", *Sandia technical memorandum*, September 12, 2000.

Moffat, H. and Sun, A., "A model for the degradation of an intermittent plated Au/Ni/Cu electrical connector due to the growth of corrosion products from atmospheric copper sulfidation", *Sandia technical memorandum* issued on January 22, 2004.

Moffat, H. and Sun, A., "Modification of model for pore corrosion of plated contacts", *Sandia technical memorandum* issued on August 16, 2004.

Moffat, H. and Sun, A., "Modifications to our model for the pore corrosion of plated copper contacts", *Sandia technical memorandum* issued on September 29, 2004.

Okamoto, K. and Kawai, S., "Electrical conduction and phase transition of copper sulfides", Japanese Journal of Applied Physics, Vol. 12, No. 8, p. 1130 – 1138 (1973).

Sackinger, P. A., Schunk, P. R., and Rao, R. R., A Newton-Raphson pseudo-solid domain mapping technique for free and moving boundary problems: a finite-element implementation, *J. Comp. Phys.*, **125**, p. 83-103 (1995).

Schunk, P. R., Sackinger, P. A., Rao, R. R., Chen, K. S., Cairncross, R. A., Baer, T. A., Labreche, D. A., "GOMA 2.0 - a full-Newton finite element program for free and moving boundary problems with coupled fluid/solid momentum, energy, mass, and chemical species transport: user's guide", *Sandia Technical Report* SAND97-2404 (1997).

Schunk, P. R., Sackinger, P. A., Rao, R. R., Chen, K. S., Baer, T. A., Labreche, D. A., Sun, A. C., Hopkins, M. M., Subia, S. R., Moffat, H. K., Secor, R. B., Roach, R. A., Wilkes, E. D., Noble, D. R., Hopkins, P. L., and Notz, P. K., "GOMA 4.0 - a full-Newton finite element program for free and moving boundary problems with coupled fluid/solid momentum, energy, mass, and chemical species transport: user's guide", *Sandia Technical Report* SAND2002-3204 (2002).

Sorensen, N. R., Braithwaite, J. W., and Hlava, P. F., "Atmospheric sulfidation of a diode", paper presented at the *190th Electrochemical Society Meeting*, San Antonio, TX, October 6 – 11, 1996.

Sorensen, N. R., Chen, K. S., Guilinger, T. R., Braithwaite, J. W., and Michael, J. R., "Predicting the effects of corrosion on the performance of electrical contacts", in *Electrochemical Society Proceedings* Volume 2001-22 (2001).

Sullivan, J. P., Barbour, J. C., Missert, N. A., Copeland, R. G., Mayer, T., M., and Campin, M. J., "The effects of varying humidity on copper sulfide film formation", *Sandia Technical Report*, SAND2004-0670 (2004).

Sun, A. and H.K. Moffat, "Parameter estimation of atmospheric copper sulfidation corrosion model", *Sandia technical memorandum* issued on January 29, 2003.

Sun, A. and H.K. Moffat, "Uncertainty quantification of an atmospheric corrosion model," Proceedings and presentation to the 9th ASCE Specialty Conference on Probabilistic Mechanics and Structural Reliability, July 26-28, 2004.

Tidblad, J. and Graedel, T. E., "GILDES model studies of aqueous chemistry. III. Initial SO_2-induced atmospheric corrosion of copper", *Corrosion Science*, Vol. 38, p. 2201(1996).

Tran, T. T. M., Fiaud, C., Sutter, E. M. M., and Villanova, A., "The atmospheric corrosion of copper by hydrogen sulphide in underground conditions", *Corrosion Science*, Vol. 45, p. 2787 (2003).

Wellman, G. W., "MAPVAR – a computer program to transfer solution data between finite element meshes", *Sandia Technical Report* SAND97-0466 (1999).

Appendix A

On the Verification of Goma's Capability for Modeling *Transient* Diffusion Processes Involving Dilute Solute Species and Slow Surface Chemical Reaction

This appendix is a slightly edited version of a Sandia technical memo (Chen 2000a).

Problem Description

We considered a *transient* binary diffusion process involving a surface chemical reaction at one of the boundaries. To simplify our problem, the solute species was taken to be present in very dilute amount such that convection or flow induced by diffusion of the solute species is essentially nonexistent (i.e. velocity of the binary mixture can be taken to be zero everywhere). To make the problem analytically tractable, we further considered the diffusion process as one dimensional, the surface chemical reaction as first order, and the reaction kinetics sufficiently slow so that the diffusion domain can be taken to be fixed. In short, we considered the following mathematical problem:

Governing Equation

$$\frac{\partial c}{\partial t} = D\frac{\partial^2 c}{\partial y^2} \qquad 0 \le y \le l \qquad (1).$$

Boundary Conditions

$$\frac{\partial c}{\partial y} = 0 \qquad \text{at } y = 0 \quad \text{for} \quad t > 0 \qquad (2),$$

$$-D\frac{\partial c}{\partial y} = kc \qquad \text{at } y = l \quad \text{for} \quad t > 0 \qquad (3),$$

Initial Condition

$$c = c_0 \qquad \text{at } t = 0 \quad \text{for} \quad 0 \le y \le l \qquad (4).$$

In Equations 1 – 4, c is molar concentration of the solute species in units of *moles/cm*^{3}, y coordinate along the diffusion path in unit of *cm*, t time in units of *second*, D diffusion coefficient in units of *cm*^{2}*/s*, k kinetic rate constant in units of *cm/s*, and l length of the fixed diffusion domain in units of *cm*. In Equations 1 and 3 the Fick's first law is used to relate flux of the solute-species to its gradient, which is a very good approximation for systems involving dilute solute species. In terms of practical applications, the mathematical problem as described in Equations 1 - 4 can arise from the gas-phase diffusion controlled process of atmospheric copper sulfidation.

Analytical Solution

Using the method of separation of variables, Equation 1 along with the associated boundary and initial conditions, Equations 2 - 4, was solved analytically to yield the following exact solution (cf. Crank 1975, Equation 4.50 on page 60):

$$\frac{c}{c_0} = \sum_{n=1}^{\infty} \frac{2L\cos(\beta_n \frac{y}{l}) e^{-\beta_n{}^2 \frac{Dt}{l^2}}}{(\beta_n{}^2 + L^2 + L)\cos\beta_n} \tag{5},$$

where $L(\equiv kl/D)$ is a dimensionless parameter, and β_n, the eigenvalues, are given by

$$\beta_n \tan\beta_n = L \tag{6}.$$

Values of β_n were obtained by solving Equation 6 iteratively using Newton's method:

$$\beta_n^{k+1} = \beta_n^k - \frac{(\beta_n^k)^2 \sin\beta_n^k \cos\beta_n^k - \beta_n^k L(\cos\beta_n^k)^2}{L(\cos\beta_n^k)^2 + (\beta_n^k)^2} \tag{7},$$

where superscript *k* indexes the Newton iteration. Values of β_n as computed by Equation 7 are presented in Table 1 respectively for n = 1, 2, 3,..., 50 and L = 0.0, 0.01, 0.1, 1, 10. These values of β_n agree perfectly (up to 4 decimal points) with that reported by Crank (1975, Table 4.2 on p. 379) for n = 1, 2, 3, 4, 5, 6.

Results and Discussion

Base Case

Figures 1 and 2 compare solute-species mole-fraction profiles (both spatial and temporal) computed by Goma with that given by the analytical solution in the Base Case. Physical parameters for the Base Case are: D = 0.1 cm^2/s, k = 0.1 cm/s, l = 1 cm such that L = 1 and the time constant for the process, $\tau = l^2/D$, is 10 seconds. In the Goma computation we used an evenly spaced 16-element mesh (only a single row of element in the direction normal to the diffusion path was used in order to reduce CPU time requirement, and the height of the elements was taken to be 0.02 cm) and a second-order accurate Crank-Nicholson time-integration scheme with a maximum time step of 0.1 second and an initial time step of 10^{-8} second. As shown clearly in Figures 1 and 2, Goma predictions agree with the analytical solution perfectly well – they overlap with each other and their differences are indiscernible.

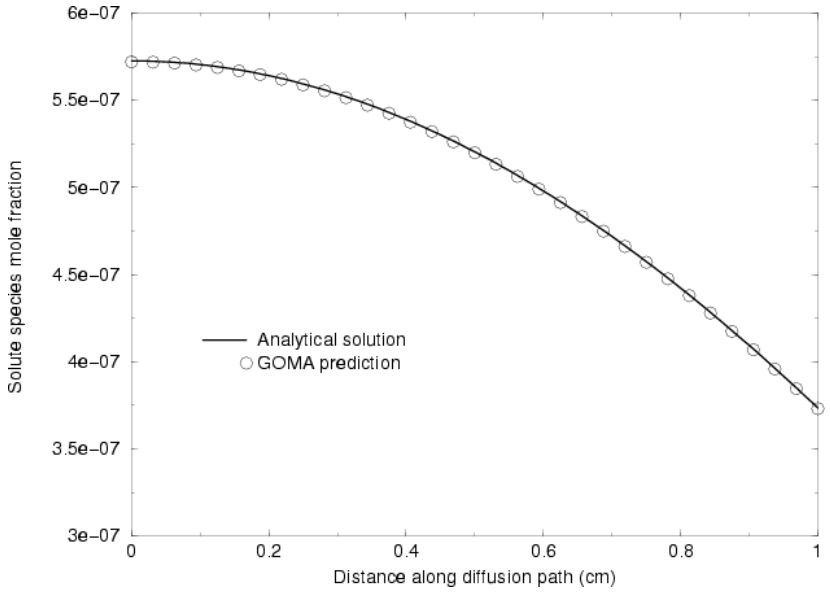

Figure 1. Comparison of Goma prediction with analytical solution – solute-species mole fraction along diffusion path at 90 seconds (16 elements along diffusion path: Crank-Nicholson time integration scheme with a maximum time step of 0.1 second).

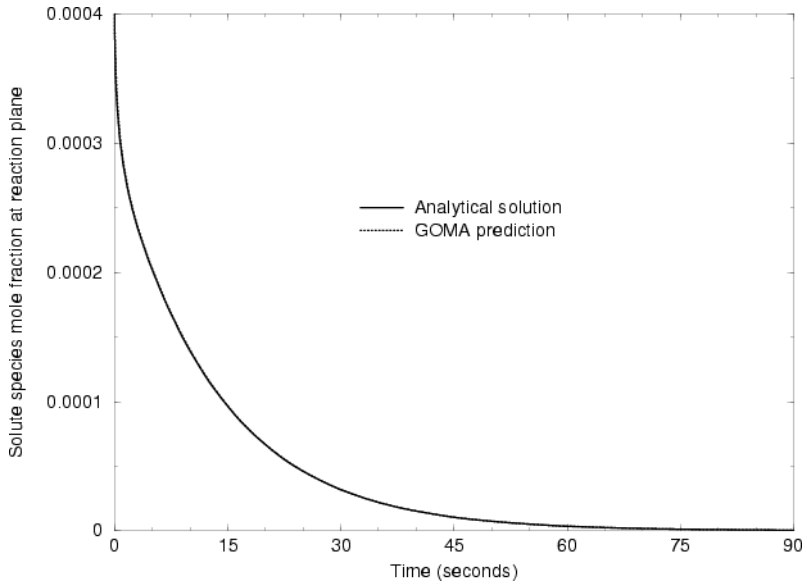

Figure 2. Comparison of Goma prediction with analytical solution – solute-species mole fraction at the reaction plane vs. time (16 elements along diffusion path: Crank-Nicholson time integration scheme with a maximum time step of 0.1 second).

Effect of Mesh Refinement

Figure 3 shows effect of mesh refinement on solute-species mole-fraction profile along diffusion path at 90 seconds as computed by Goma. The physical parameters are those in the Base Case. Here, a Crank-Nicholson time integration scheme with a maximum time step of 0.1 second was used in computing the Goma results. Also displayed is that given by the analytical solution. As shown, a two-element (quadratic, evenly spaced) mesh actually does a pretty good job already as compared with the analytical solution. As the mesh density increases (i.e. from 2 elements to 4 elements to 8 elements, etc.), the differences between Goma prediction and the analytical solution become less discernible, as expected. In fact, an eight-element (quadratic, evenly spaced) mesh yielded Goma prediction that is essentially indiscernible from the analytical solution. To ensure solution accuracy, we employed a 16-element (quadratic, evenly spaced) mesh in the Base Case and the Goma computations discussed below.

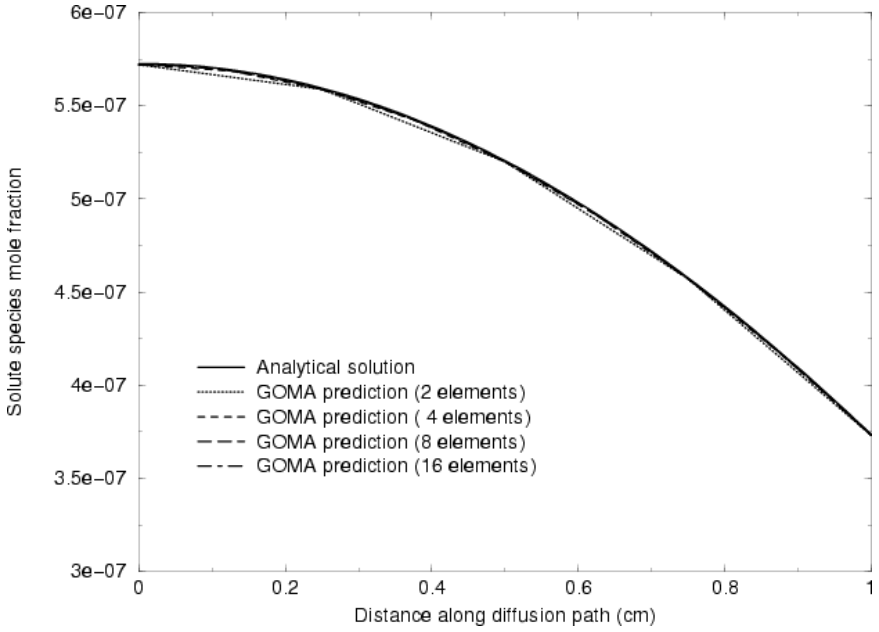

Figure 3. Effect of mesh refinement on Goma prediction – solute-species mole fraction along diffusion path at 90 seconds (Crank-Nicholson time integration scheme with a maximum time step of 0.1 second).

Effect of Time-Integration Scheme

Figure 4 displays effect of time-integration scheme (*Crank-Nicholson* vs. *backward Euler*) on solute-species mole-fraction profile along diffusion path at 90 seconds. The physical parameters are those in the Base Case. As expected, the second-order accurate *Crank-Nicholson* scheme yields better accuracy as compared with the first-order accurate *backward Euler* method: the Goma prediction obtained using the *Crank-Nicholson* scheme agrees perfectly well with the analytical solution whereas discrepancy between the Goma prediction obtained using the *backward Euler* method and the analytical solution obviously exists.

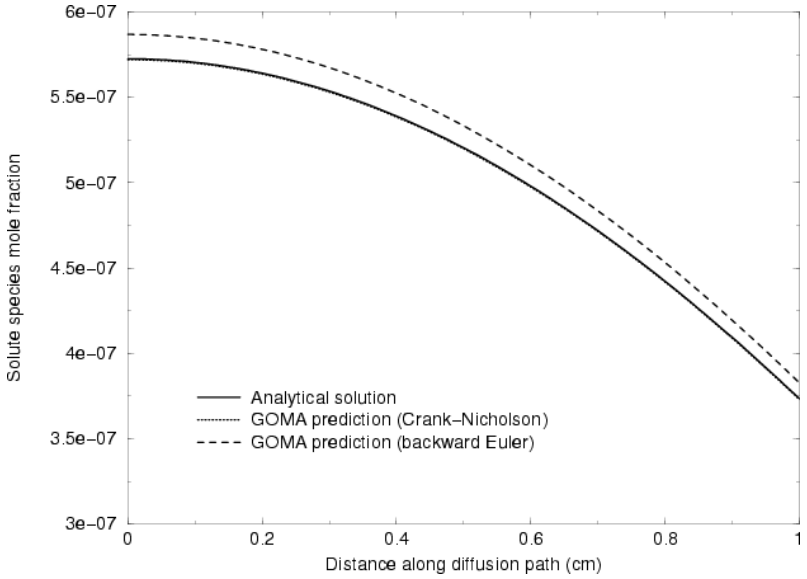

Figure 4. Effect of time-integration scheme on Goma prediction – solute-species mole fraction along diffusion path at 90 seconds (16 elements, maximum time step = 0.1 second).

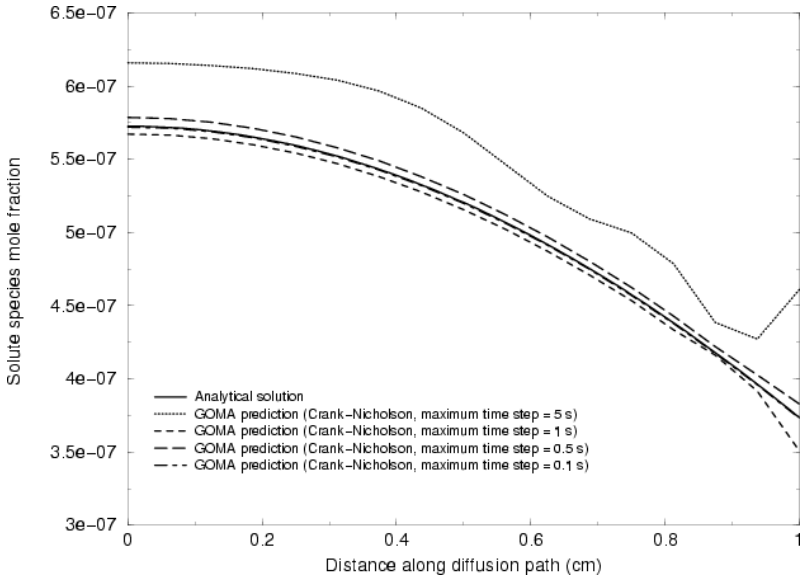

Figure 5. Effect of maximum time step on Goma prediction – solute-species mole fraction along diffusion path at 90 seconds (16 elements, Crank-Nicholson time integration scheme).

Effect of Maximum Time Step

Figures 5 and 6 show the effects of *maximum time step* allowed in Goma computations on solute-species mole-fraction profiles, respectively, along diffusion path at 90 seconds and

at the reaction plane as a function of time. The physical parameters are those in the Base Case. Clearly, the Goma predictions agree perfectly with the analytical solution results only when the *maximum time step* allowed is sufficiently small, e.g. 0.1 second. As presented in Figure 7, CPU time required increases exponentially with decreasing *maximum time step* allowed when it becomes desirably small.

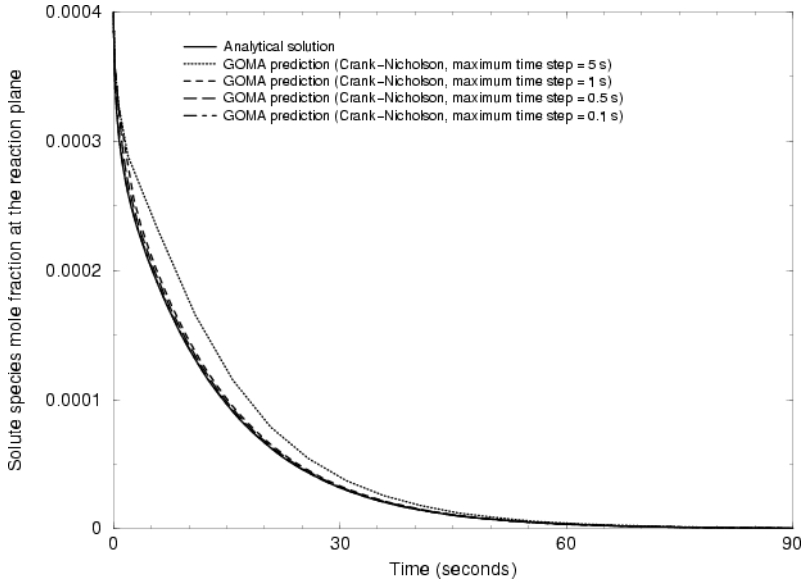

Figure 6. Effect of maximum time step on Goma prediction – solute-species mole fraction at reaction plane as a function of time (16 elements, Crank-Nicholson time integration scheme).

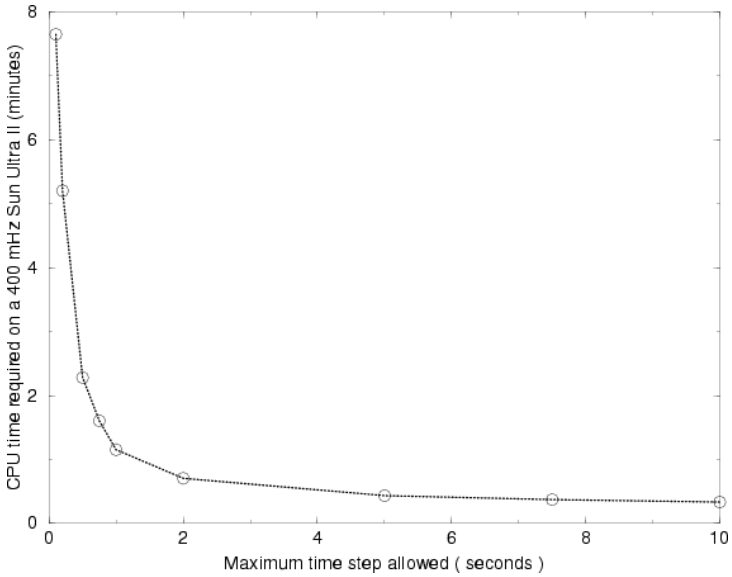

Figure 7. CPU time required as a function of maximum time step allowed (16 elements, Crank-Nicholson time integration scheme, tim = 90 s).

Effect of Not Specifying Maximum Time Step

As displayed in Figures 8 and 9, significantly incorrect Goma predictions were obtained when the *maximum time step* parameter was not specified (that is, the *maximum time step* card was absent in the input file) and the *time step error* parameter was set to 0.01. Though the computed Goma results may appear to be smooth as in Figure 8, they are incorrect (off by more than an order of magnitude) as compared with the analytical solution. Here, the physical parameters are those in the Base Case.

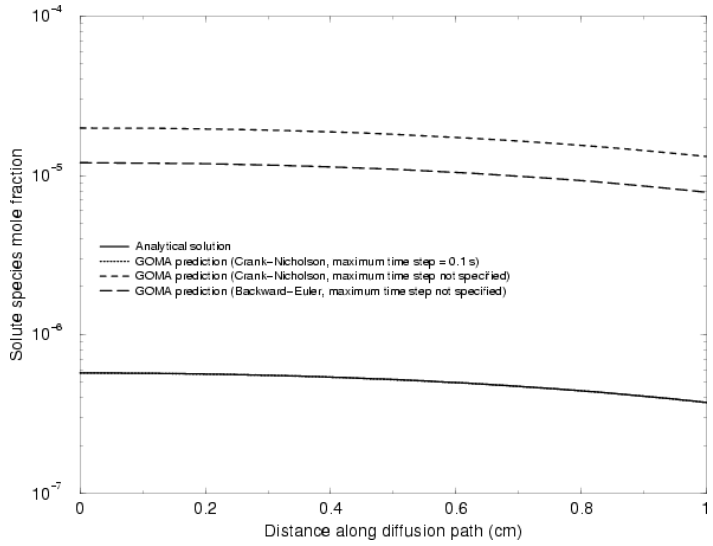

Figure 8. Effect of not specifying a maximum time step on Goma prediction – Solute-species mole fraction along diffusion path at 90 seconds (16 elements, Crank-Nicholson time integration scheme).

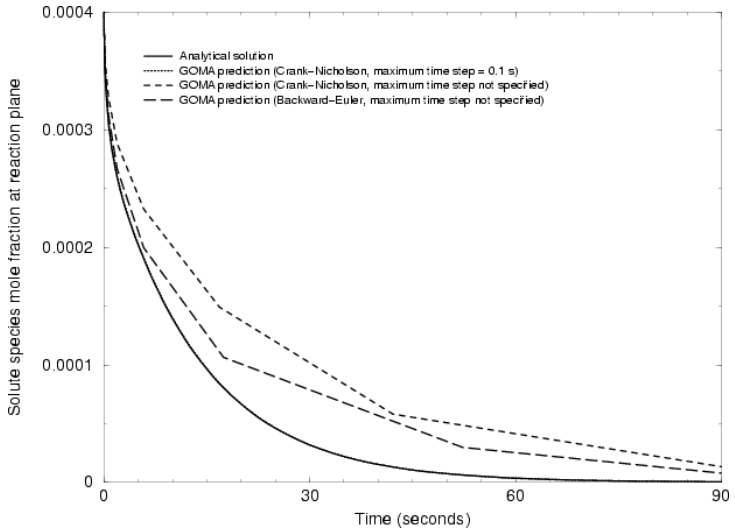

Figure 9. Effect of not specifying maximum time step on Goma prediction – solute-species mole fraction at reaction plane as a function of time (16 elements, Crank-Nicholson time integration scheme).

Effect of Time Step Error

When the *maximum time step* parameter is not specified, the time-integration errors can be controlled to a certain extent by the *time step error* parameter. When negative, the absolute value of the *time step error* parameter measures the percentage error in the time-integration error norm whereas it indicates the absolute value of the norm when positive. Figures 10a and 10b show effects of *time step error* on solute-species mole-fraction profile along diffusion path at 90 seconds, respectively, for the cases of negative and positive *time step error*. The physical parameters are those in the Base Case. As shown in Figure 10a, when the *time step error* parameter is negative, the smaller its absolute value the more accurate of the computed Goma prediction, which is as expected since the percentage error becomes smaller. As shown in Figure 11, there is a price to pay, however, in terms of CPU time requirement as the percentage error is reduced: CPU time increases exponentially as the absolute value of time step error decreases, particularly to desirably small values (e.g. 0.0001 or less).

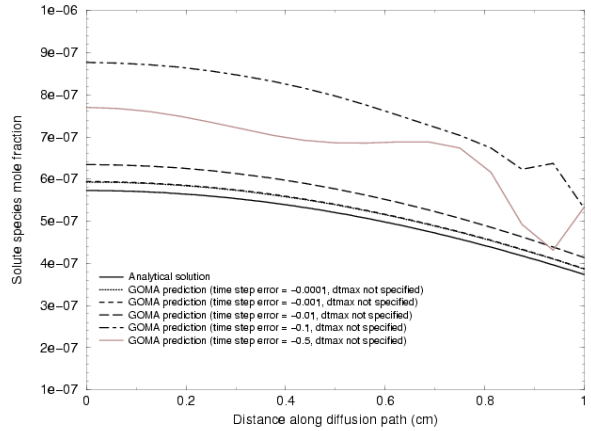

Figure 10a. Effect of time step error (negative values) on Goma prediction – solute-species mole fraction along diffusion path at 90 seconds (16 elements, Crank-Nicholson time integration scheme).

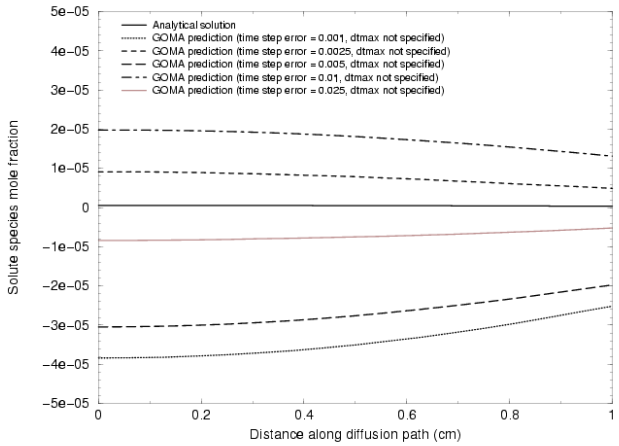

Figure 10b. Effect of time step error (positive values) on Goma prediction – solute-species mole fraction along diffusion path at 90 seconds (16 elements, Crank-Nicholson time integration scheme).

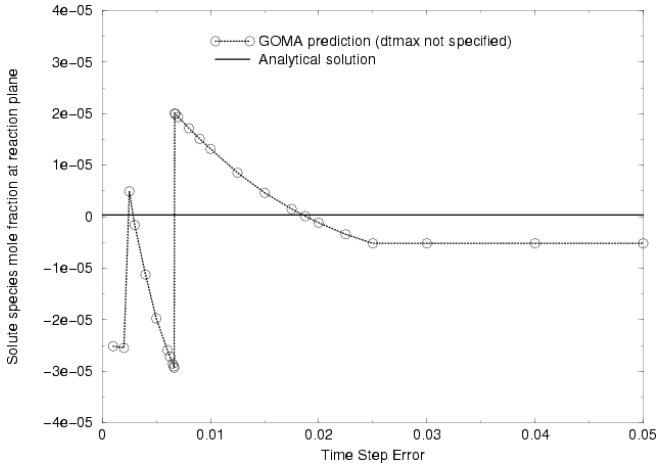

Figure 10c. Effect of time step error (positive values) on Goma prediction – solute-species mole fraction at reaction plane at 90 seconds (16 elements, Crank-Nicholson time integration scheme).

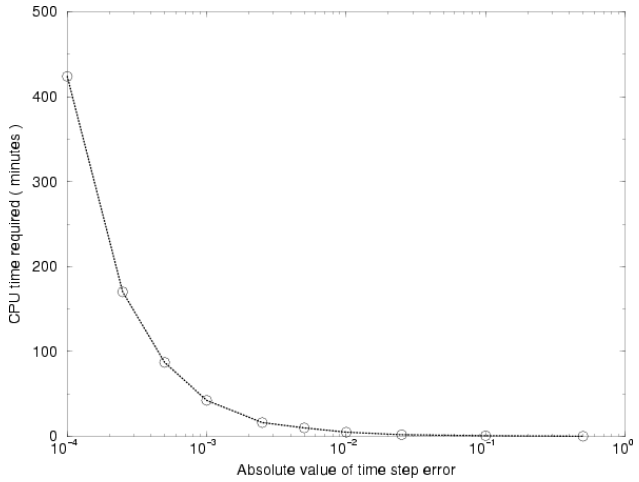

Figure 11. CPU time required as a function of absolute value of time step error (for the case of negative time step error, 16 elements, Crank-Nicholson time integration scheme, time = 90 s).

Figures 10b and 10c show the effects of *time step error* when its value is positive. In this case, no clear trend (in terms of reducing discrepancy between Goma prediction and analytical solution) can be observed, suggesting that *time step error* when positive is <u>not</u> a good parameter for controlling time integration errors.

<u>Effect of Initial Time Step</u>

Figures 12 and 13 show effects of *initial time step* on the computed Goma predictions of solute-species mole fraction. The physical parameters are those in the Base Case. As expected, effect of the *initial time step* is small for the range of values studied.

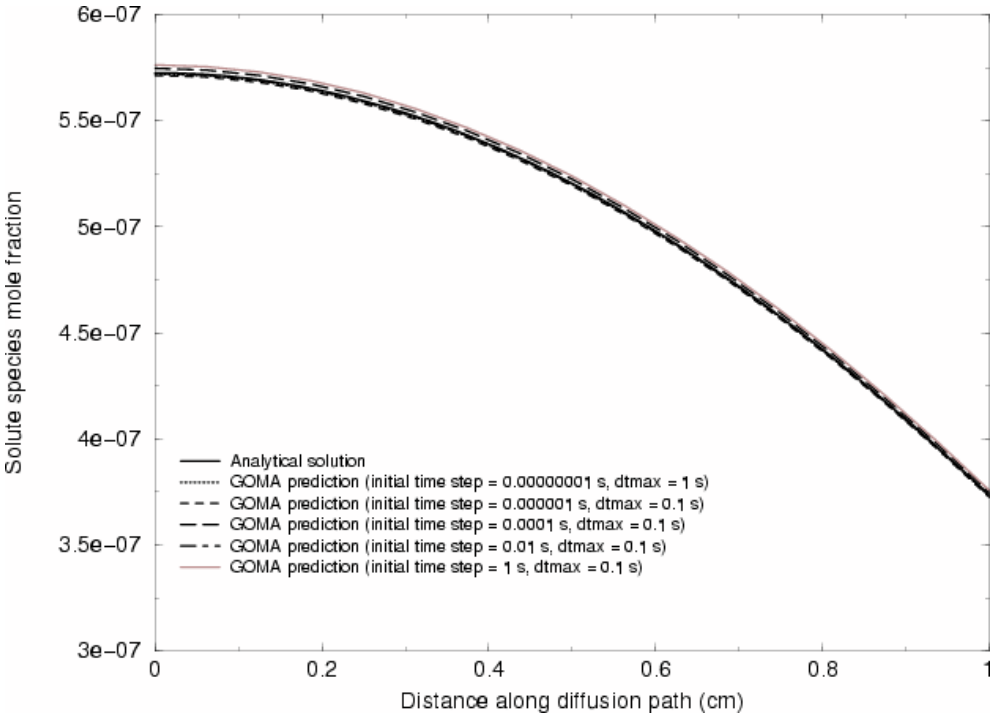

Figure 12. Effect of initial time step on Goma prediction – solute-species mole fraction along diffusion path at 90 seconds (16 elements, Crank-Nicholson time integration scheme).

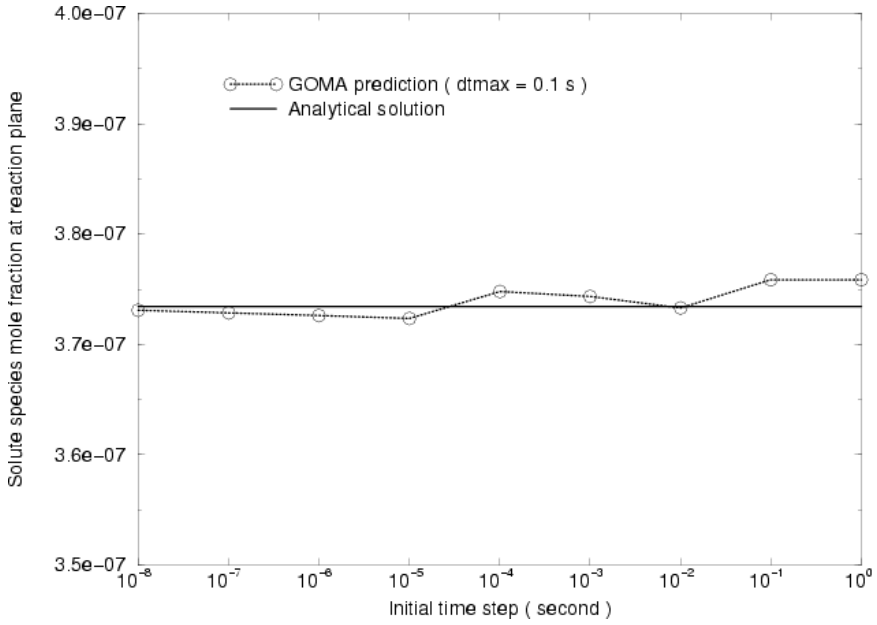

Figure 13. Effect of initial time step on Goma prediction – solute-species mole fraction at reaction plane at 90 seconds (16 elements, Crank-Nicholson time integration scheme).

Summary and Conclusions

For the first time, effects of time-integration scheme and parameters on Goma predictions was systematically studied using a time-dependent model problem for which analytical solution can be obtained. The model problem involves a diffusion process with a dilute solute species and a slow surface chemical reaction at one of the boundaries. It was found that Goma predictions of solute-species concentration profiles agree perfectly well with that given by the analytical solution when proper time-integration scheme and parameters were employed. When inappropriate time-integration scheme or parameters were used, however, significantly incorrect results were obtained. As expected, the second-order accurate Crank-Nicholson time-integration scheme yielded more accurate predictions as compared with the first-order accurate backward-Euler method. Of the parameters used by Goma in time integration, the *maximum-time-step* parameter was found to be most effective in reducing time-integration errors. As a rule of thumb, the maximum time step allowed should be less than the time constant of the process, based on the limited findings in the case study reported here. Lastly, effect of mesh refinement was also examined and it was found that in modeling transient processes errors resulted from inappropriate use of time integration scheme and parameters are much more significant than that from the employment of an inadequately refined mesh (that is, errors from time integration are much more pronounced than that from mesh refinement) based, again, on limited findings presented in this appendix.

References

Crank, J., The Mathematics of Diffusion, Second Edition, Oxford University Press, New York, NY (1975).

Table 1. Roots of $\beta_n \tan \beta_n = L$ for n = 1, 2, 3,..., 50 and Various Values of L

n	$L = 0$	$L = 0.01$	$L = 0.1$	$L = 1$	$L = 10$
1	0.00000	0.09983	0.31105	0.86033	1.42887
2	3.14159	3.14477	3.17310	3.42562	4.30580
3	6.28319	6.28478	6.29906	6.43730	7.22811
4	9.42478	9.42584	9.43538	9.52933	10.20030
5	12.56640	12.56720	12.57430	12.64530	13.21420
6	15.70800	15.70860	15.71430	15.77130	16.25940
7	18.84960	18.85010	18.85490	18.90240	19.32700
8	21.99110	21.99160	21.99570	22.03650	22.41080
9	25.13270	25.13310	25.13670	25.17240	25.50640
10	28.27430	28.27470	28.27790	28.30960	28.61060
11	31.41590	31.41620	31.41910	31.44770	31.72130
12	34.55750	34.55780	34.56040	34.58640	34.83710
13	37.69910	37.69940	37.70180	37.72560	37.95670
14	40.84070	40.84090	40.84320	40.86520	41.07950
15	43.98230	43.98250	43.98460	44.00500	44.20480
16	47.12390	47.12410	47.12600	47.14510	47.33210
17	50.26550	50.26570	50.26750	50.28540	50.46110
18	53.40710	53.40730	53.40890	53.42580	53.59160
19	56.54870	56.54880	56.55040	56.56630	56.72320
20	59.69030	59.69040	59.69190	59.70700	59.85580
21	62.83190	62.83200	62.83340	62.84780	62.98930
22	65.97340	65.97360	65.97500	65.98860	66.12350
23	69.11500	69.11520	69.11650	69.12950	69.25840
24	72.25660	72.25680	72.25800	72.27050	72.39390
25	75.39820	75.39840	75.39950	75.41150	75.52990
26	78.53980	78.53990	78.54110	78.55250	78.66630
27	81.68140	81.68150	81.68260	81.69360	81.80310
28	84.82300	84.82310	84.82420	84.83480	84.94020
29	87.96460	87.96470	87.96570	87.97600	88.07760
30	91.10620	91.10630	91.10730	91.11720	91.21540
31	94.24780	94.24790	94.24880	94.25840	94.35340
32	97.38940	97.38950	97.39040	97.39960	97.49160
33	100.53100	100.53100	100.53200	100.54100	100.63000
34	103.67300	103.67300	103.67400	103.68200	103.76900
35	106.81400	106.81400	106.81500	106.82400	106.90700
36	109.95600	109.95600	109.95700	109.96500	110.04600
37	113.09700	113.09700	113.09800	113.10600	113.18500
38	116.23900	116.23900	116.24000	116.24800	116.32500
39	119.38100	119.38100	119.38100	119.38900	119.46400
40	122.52200	122.52200	122.52300	122.53000	122.60300
41	125.66400	125.66400	125.66500	125.67200	125.74300
42	128.80499	128.80499	128.80600	128.81300	128.88300
43	131.94701	131.94701	131.94800	131.95399	132.02200
44	135.08800	135.08900	135.08900	135.09599	135.16200
45	138.23000	138.23000	138.23100	138.23700	138.30200
46	141.37199	141.37199	141.37199	141.37900	141.44200
47	144.51300	144.51300	144.51401	144.52000	144.58200
48	147.65500	147.65500	147.65601	147.66200	147.72200
49	150.79601	150.79700	150.79700	150.80299	150.86301
50	153.93800	153.93800	153.93900	153.94501	154.00301

Appendix B.

On the Verification of Goma Baseline Model for Atmospheric Copper Sulfidation in the Gas-phase-Diffusion Controlled Regime with Fixed Sulfidation-Front Approximdation

This appendix is a slightly edited version of a Sandia technical memo (Chen 2000b).

Problem Description

A baseline multi-dimensional mathematical model of copper sulfidation for the initial implementation in Goma was documented by the author in an earlier communication (Chen, 1999). Readers who are interested in a more detailed description of the physical phenomena involved in atmospheric sulfidation of copper by hydrogen sulfide are referred to the Sandia Report by Larson (1998) and references cited therein. To facilitate the verification of the Goma model, we considered the sulfidation process as gas-phase diffusion controlled, i.e., the rate of sulfidation depends only on the local concentration of the sole solute species, H_2S, which diffuses in the stagnant air. To simplify our problem, the solute species was taken to be present in very dilute amount (on the order of hundreds of *part per million* or less) such that convection or flow induced by diffusion of the solute species is essentially nonexistent (i.e. velocity of the binary mixture can be taken to be zero everywhere). To make the problem analytically tractable, we further considered the diffusion process as one dimensional, the surface sulfidation reaction as first order, and the reaction kinetics sufficiently slow so that the gas-phase diffusion domain can be taken to be fixed. Actually, the fixed-domain approximation can be justified by the fact that the solute species, H_2S, is present only in very low concentration (on the order of hundreds of *part per million* or less); more specifically, the gas-phase domain is on the order a centimeter whereas the sulfide growth layer thickness is on the order of a micron, which makes the reduction in diffusion domain length essentially nonexistent. Mathematically, the problem can be stated as follow:

Governing Equation

$$\frac{\partial c_{H_2S}}{\partial t} = D\frac{\partial^2 c_{H_2S}}{\partial y^2} \qquad 0 \le y \le l \qquad (1).$$

Boundary Conditions

$$\frac{\partial c_{H_2S}}{\partial y} = 0 \qquad \text{at } y = 0 \quad \text{for} \quad t > 0 \qquad (2),$$

$$-D\frac{\partial c_{H_2S}}{\partial y} = k c_{H_2S} \qquad \text{at } y = l \quad \text{for} \quad t > 0 \qquad (3),$$

Initial Condition

$$c_{H_2S} = c_{H_2S,0} \qquad \text{at } t = 0 \quad \text{for} \quad 0 \le y \le l \qquad (4).$$

In above c_{H_2S} is the molar concentration of H_2S in units of *moles/cm*^{3}, *y* coordinate along the diffusion path in units of *cm*, *t* time in units of *second*, *D* diffusion coefficient in units of *cm*^{2}*/s*, *k* first-order kinetic rate constant in units of *cm/s*, and *l* length of the fixed diffusion domain in units of *cm*. In Equations 1 and 3 the Fick's first law is used to relate flux of the solute-species to its gradient, which is a very good approximation for systems involving dilute solute species. Equation 2 simply states that there is no flux of H_2S across the non-reacting boundary (i.e., y = 0). This was chosen so that the analytical solution can be cleanly obtained. Another possibility is to specify the concentration of H_2S at y = 0. Actually, a more general or appropriate boundary condition at y = 0 is to specify a non-zero flux by using a mass-transfer coefficient, α:

$$\frac{\partial c_{H_2S}}{\partial y} = \alpha(c_{H_2S} - c_{H_2S,b}) \qquad \text{at} \quad y = 0 \quad \text{for} \quad t > 0 \qquad (5),$$

where $c_{H_2S,b}$ is the concentration of H_2S in the bulk (i.e., outside the boundary at y = 0). In this case, the additional parameter needed to be specified is the mass-transfer coefficient, α, which depends on the location of the boundary at y = 0.

Analytical Solution

As shown in Appendix A, Equation 1 along with the associated boundary and initial conditions, Equations 2 - 4, can be solved analytically using the method of separation of variables to yield the following exact solution (cf. Crank 1975, Equation 4.50 on page 60):

$$\frac{c}{c_0} = \sum_{n=1}^{\infty} \frac{2L\cos(\beta_n \frac{y}{l}) e^{-\beta_n{}^2 \frac{Dt}{l^2}}}{(\beta_n{}^2 + L^2 + L)\cos\beta_n} \qquad (6),$$

where $L(\equiv kl/D)$ is a dimensionless parameter, and β_n, the eigenvalues, are given by

$$\beta_n \tan\beta_n = L \qquad (7).$$

Values of β_n can be obtained by solving Equation 7 iteratively using Newton's method and they are listed in Table 1 of Appendix A for *n* = 1, 2, 3, …, 50 and *L* = 0.0, 0.01, 0.1, 1, 10.

From the mass balance on copper sulfide (Cu_2S), we have

$$\frac{d\rho_{Cu_2S} hA}{dt} = M_{Cu_2S} r_{Cu_2S} A \qquad (8),$$

where A is total area of the copper-substrate surface on which sulfidation occurs in units of cm^2, h the average thickness of the dense copper sulfide layer in unit of cm, ρ_{Cu_2S} density of copper sulfide in units of g/cm^3, M_{Cu_2S} molecular weight of copper sulfide in units of $g/mole$, and r_{Cu_2S} the rate of formation of copper sulfide in units of $mole/cm^2\text{-}s$. From stoichiometry of the overall copper sulfidation reaction (cf. Larson 1998),

$$2Cu + H_2S(g) + \frac{1}{2}O_2(g) \quad \rightarrow \quad Cu_2S + H_2O(l) \qquad (9),$$

we have $r_{Cu_2S} = r_{H_2S}$ where r_{H_2S} is the rate of consumption of H_2S; that is, the rate of formation of Cu_2S is equal to the rate of consumption of H_2S. Upon substitution, Equation 8 becomes

$$\frac{d\rho_{Cu_2S}h}{dt} = M_{Cu_2S}r_{Cu_2S} \qquad (10).$$

With the first-order kinetics assumption stated previously, we have

$$r_{H_2S} = kc_{H_2S}\Big|_{y=l} = kcx_{H_2S}\Big|_{y=l} \qquad (11),$$

where c is the total molar concentration of the air/H_2S mixture and can be determined using the ideal gas law (i.e., $c = \frac{p}{RT}$; under normal condition of 1 atm and 25^oC, c = 4.09x10^{-5} mol/cm^3), x_{H_2S} the mole fraction of H_2S. Combining Equations 10 and 11 yields

$$\frac{dh}{dt} = \frac{cM_{Cu_2S}}{\rho_{Cu_2S}}kx_{H_2S}\Big|_{y=l} \qquad (12).$$

From Equation 6, we have

$$\frac{x_{H_2S}}{x_{H_2S,0}} = \sum_{n=1}^{\infty}\frac{2Le^{-\beta_n^2\frac{Dt}{l^2}}}{(\beta_n^2 + L^2 + L)} \qquad (13).$$

Upon substituting Equation 13 into Equation 12 and subsequently integrating with the initial condition of h = 0 at t = 0, we obtain the average copper sulfide layer thickness as a function of time:

$$\frac{h(t)}{l} = \frac{2cM_{Cu_2S}}{\rho_{Cu_2S}} x_{H_2S,0} L^2 \sum_{n=1}^{\infty} \frac{\left(1 - e^{-\beta_n{}^2 \frac{Dt}{l^2}}\right)}{(\beta_n{}^2 + L^2 + L)\beta_n{}^2} \qquad (14).$$

Goma Model Computation

Equation 1 along with boundary and initial conditions as specified in Equations 2 - 4 was solved using Goma to yield x_{H_2S} as a function of time and spatial position. In the Goma computation we used an evenly spaced 16-element mesh (only a single row of element in the direction normal to the diffusion path was used in order to reduce CPU time requirement, and the height of the elements was taken to be 0.02 cm) and a second-order accurate Crank-Nicholson time-integration scheme with an initial time step of 10^{-9} second. Effects of mesh refinement and time-integration scheme and parameters for this problem have been studied and is documented in Appendix A. After computed x_{H_2S} with Goma, we integrated Equation 12 numerically using Trapezoidal rule to yield the average thickness of the copper sulfide layer at discrete time steps:

$$h(t_i) = h(t_{i-1}) + \frac{cM_{Cu_2S}}{\rho_{Cu_2S}} k[x_{H_2S}(t_i)\big|_{y=l} + x_{H_2S}(t_{i-1})\big|_{y=l}] \qquad (15).$$

Results and Discussion

Comparisons of Goma prediction with analytical solution are presented in Figures 1 and 2, respectively, for H_2S solute species mole fraction on the sulfidation surface and average sulfide layer thickness as functions of time under two different sets of transport/kinetic properties and process condition. Clearly, the Goma predictions agree perfectly well with the results from the analytical solution.

Effects of maximum time step allowed in Goma computations on H_2S solute species mole fraction on the sulfidation surface and average sulfide layer thickness are presented in Figures 3 and 4, again, for two different sets of transport/kinetic properties and process condition. When maximum time steps are sufficiently small, excellent agreements are seen between Goma predictions and results from the analytical solution. When the maximum time steps exceed threshold values, discrepancies arise, and they are significant when the maximum time steps become relatively large. The effect of maximum time step on average sulfide layer thickness is more pronounced than that on H_2S solute species mole fraction because the maximum time step further contributes to the discrepancy in the numerical integration step that yields the average sulfide layer thickness once x_{H_2S} is computed.

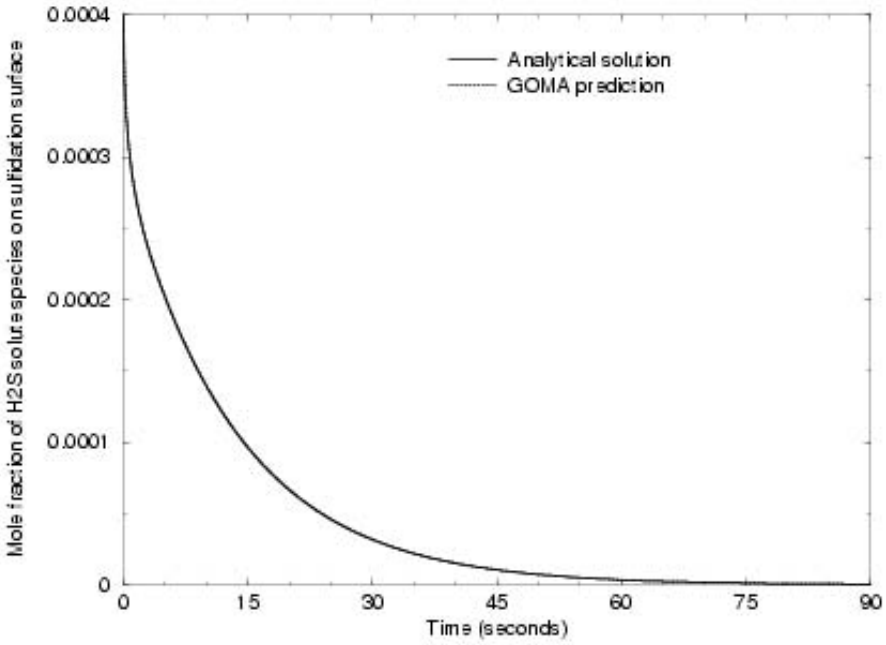

Figure 1a. Comparison of Goma prediction with analytical solution – H_2S solute-species mole fraction on the sulfidation surface as a function of time. (parameters: $D = 0.1$ cm^2/s, $k = 0.1$ cm/s, $l = 1$ cm, $x_{H_2S,0} = 400$ ppm; Crank-Nicholson scheme with a maximum time step of 0.05 second).

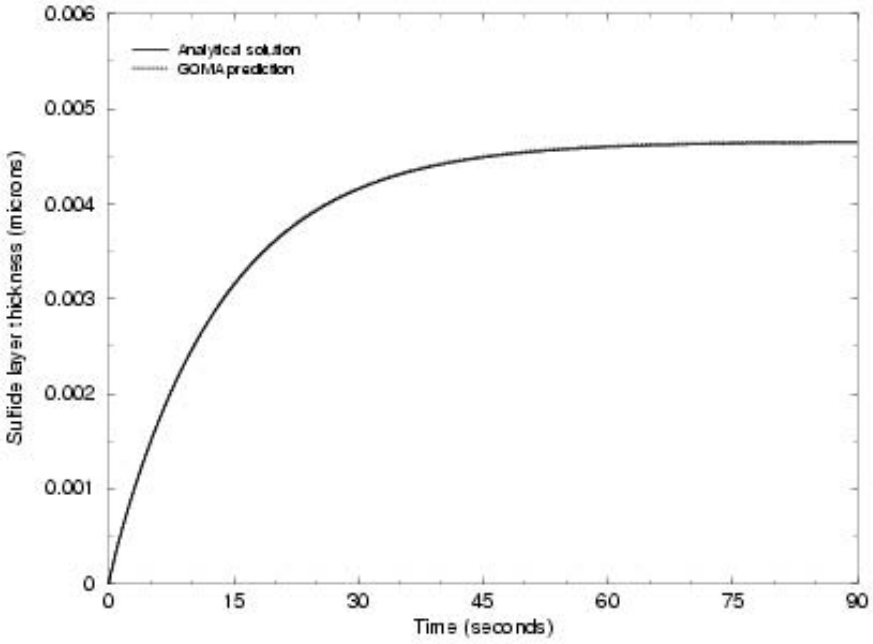

Figure 1b. Comparison of Goma prediction with analytical solution – average sulfide layer thickness as a function of time . (parameters: $D = 0.1$ cm^2/s, $k = 0.1$ cm/s, $l = 1$ cm, $x_{H_2S,0} = 400$ ppm; Crank-Nicholson scheme with a maximum time step of 0.05 second).

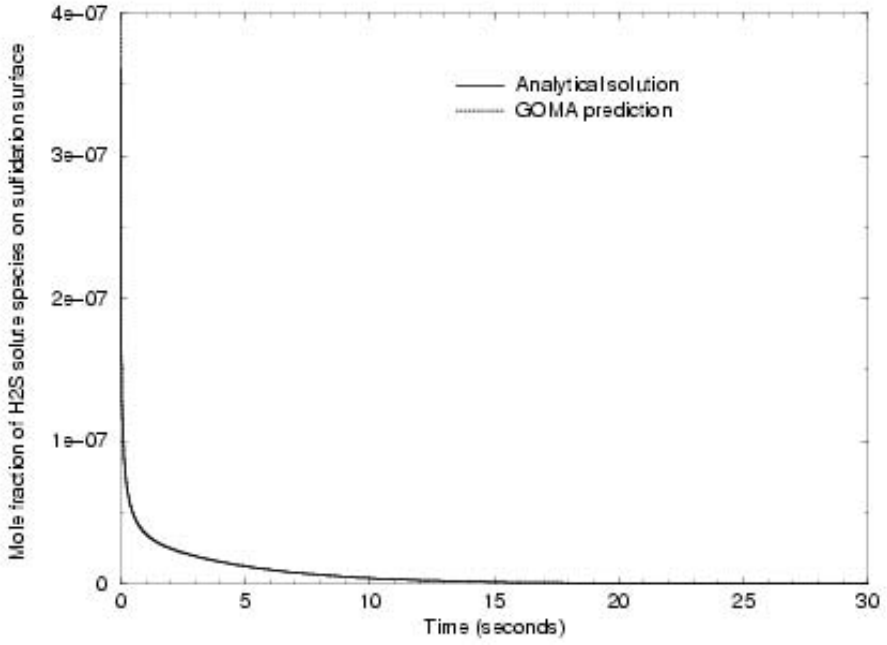

Figure 2a. Comparison of Goma prediction with analytical solution – H_2S solute-species mole fraction on the sulfidation surface as a function of time. (parameters: D = 0.1 cm^2/s, k = 2 cm/s, l = 1 cm, $x_{H_2S,0}$ = 400 ppb; Crank-Nicholson scheme with a maximum time step of 0.005 second).

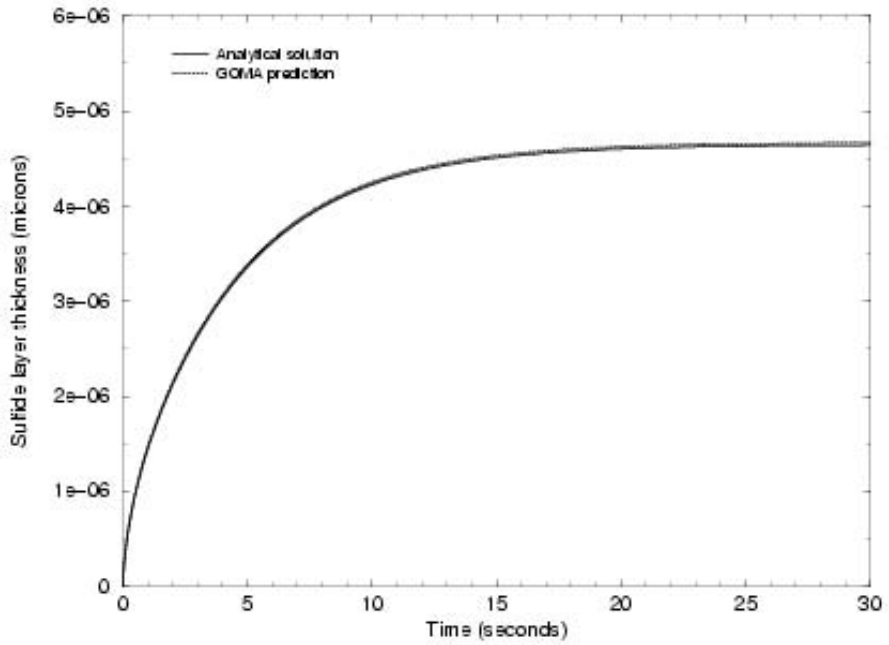

Figure 2b. Comparison of Goma prediction with analytical solution – average sulfide layer thickness as a function of time . (parameters: D = 0.1 cm^2/s, k = 2 cm/s, l = 1 cm, $x_{H_2S,0}$ = 400 ppb; Crank-Nicholson scheme with a maximum time step of 0.005 second).

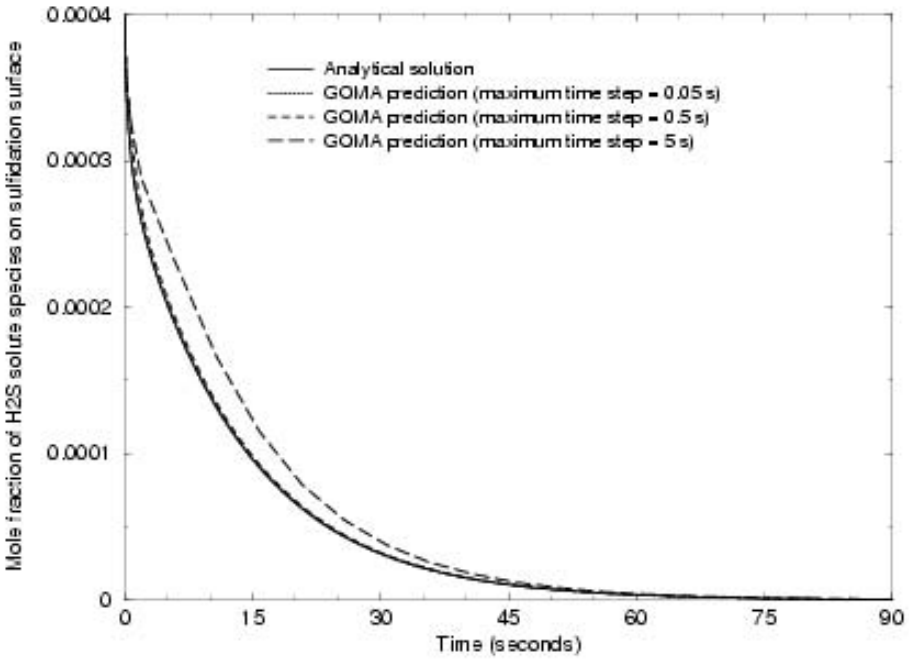

Figure 3a. Effect of maximum time step on Goma prediction – H_2S solute-species mole fraction on the sulfidation surface as a function of time. (parameters: $D = 0.1$ cm^2/s, $k = 0.1$ cm/s, $l = 1$ cm, $x_{H_2S,0} = 400$ ppm; Crank-Nicholson time-integration scheme).

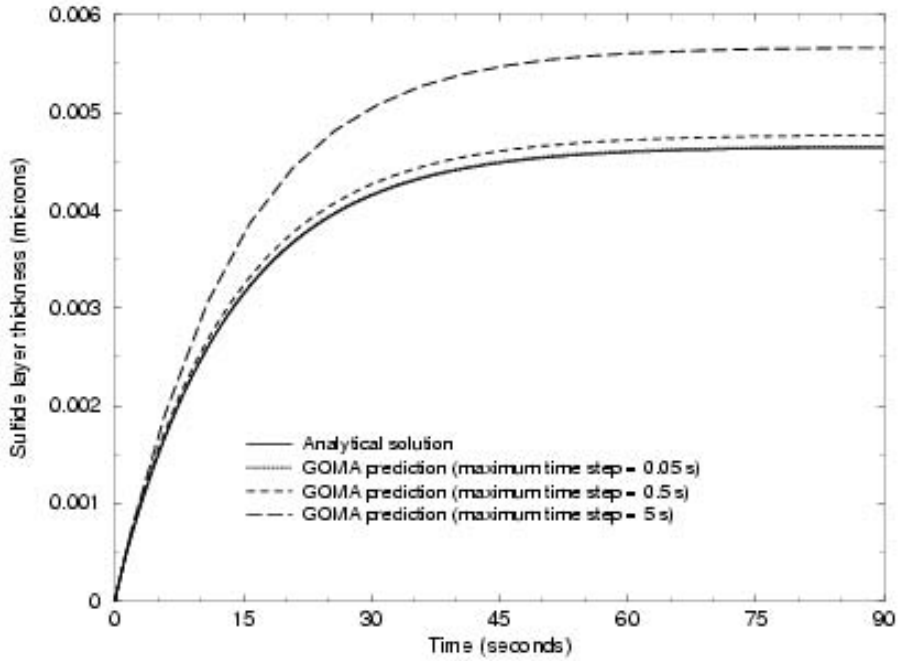

Figure 3b. Effect of maximum time step on Goma prediction – average sulfide layer thickness as a function of time . (parameters: $D = 0.1$ cm^2/s, $k = 0.1$ cm/s, $l = 1$ cm, $x_{H_2S,0} = 400$ ppm; Crank-Nicholson time-integration scheme).

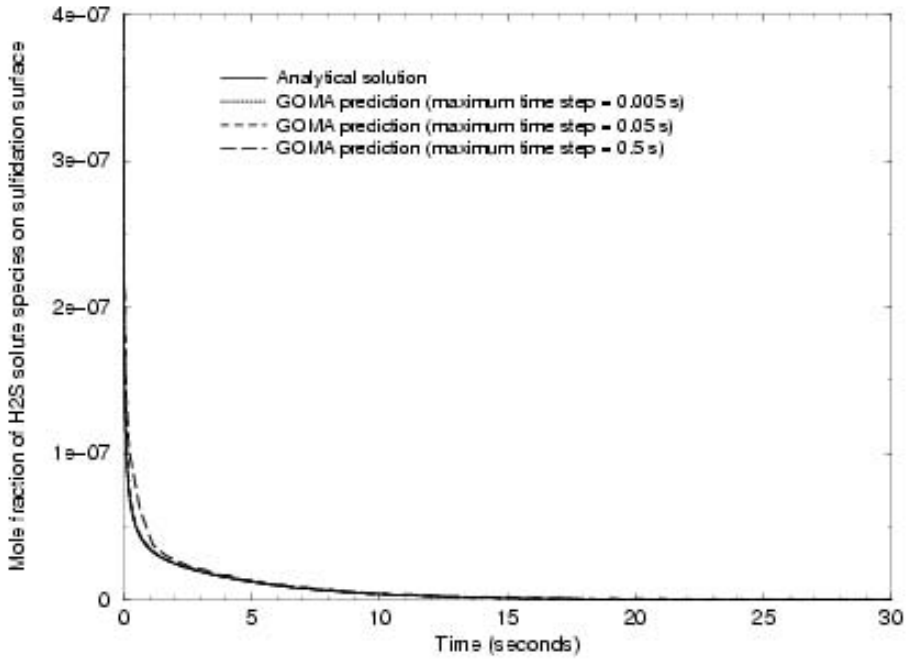

Figure 4a. Effect of maximum time step on Goma prediction – H_2S solute-species mole fraction on the sulfidation surface as a function of time. (parameters: D = 0.1 cm^2/s, k = 2 cm/s, l = 1 cm, $x_{H_2S,0}$ = 400 ppb; Crank-Nicholson time-integration scheme).

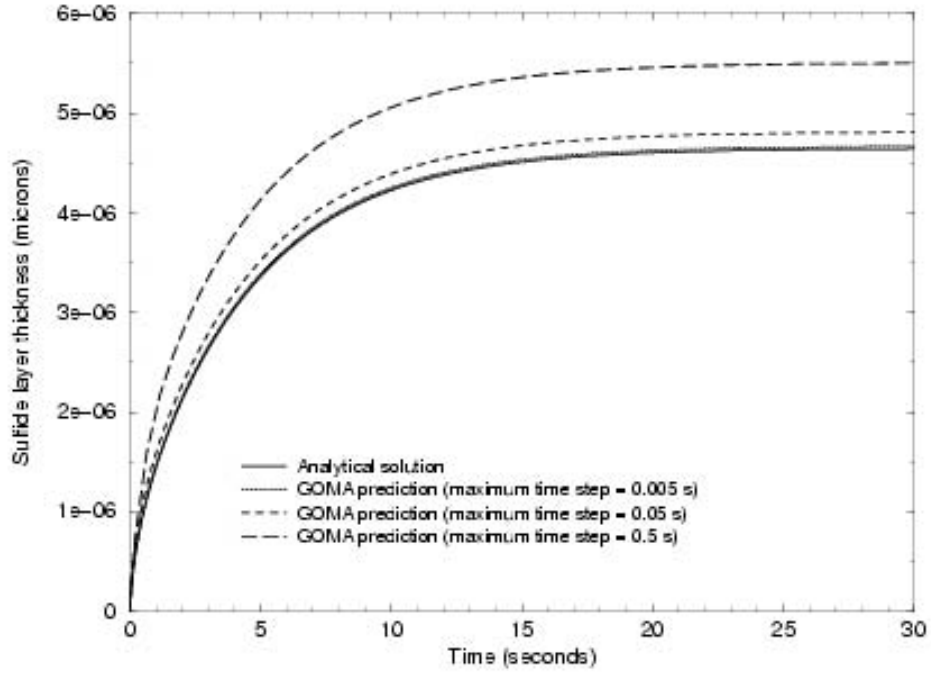

Figure 4b. Effect of maximum time step on Goma prediction – average sulfide layer thickness as a function of time . (parameters: D = 0.1 cm^2/s, k = 2 cm/s, l = 1 cm, $x_{H_2S,0}$ = 400 ppb; Crank-Nicholson time-integration scheme).

The verified Goma model was employed to study effects of the boundary condition at the outer non-reacting boundary on H_2S solute species mole fraction on the sulfidation surface and average sulfide layer thickness, and the results are shown in Figures 5 and 6. As expected, the boundary condition of no-mass across the non-reacting boundary gave rise to an equilibrium average sulfide layer thickness because all the H_2S solute initially present in the domain was eventually consumed completely. On the other hand, the boundary condition of constant H_2S concentration at the outer non-reacting boundary yields a linearly increasing average sulfide layer thickness at steady state because H_2S solute species mole fraction on the sulfidation surface achieves an equilibrium value once steady state is reached. It is informative that the two different boundary conditions (zero species-mass flux vs. constant species concentration) yield the same sulfide layer thickness at short times.

To demonstrate its utility, the verified Goma model was exercised to compute prediction of the average sulfide layer thickness for a couple of hours of sulfidation using realistic transport/kinetic properties and process conditions (D = 0.1 cm^2/s, k = 2 cm/s, $x_{H_2S,0}$ = 400 ppb), and the boundary condition of constant H_2S solute species concentration on the outer non-reacting surface ($x_{H_2S,0}$ = 400 ppb at y = 0). The result is displayed in Figure 7. For the time scale shown, sulfide layer thickness increases essentially linearly with time. At short times, however, the growth rate of the sulfide layer decreases with time as can be seen in Figure 6b.

Summary and Conclusion

This memorandum documents a case study of verifying a Goma baseline model for atmospheric copper sulfidation in the gas-phase-diffusion controlled regime with the fixed sulfidation-front approximation. Excellent agreement was found between Goma predictions (H_2S solute species concentration profiles and sulfide growth layer thickness) and results from the analytical solution. Effects of maximum time step allowed in Goma on H_2S solute species concentration profiles and sulfide growth layer thickness were examined and found to be significant (particularly when the maximum time steps are large). After verification, the Goma model was employed to study the effects of the boundary condition at the outer non-reacting surface on H_2S solute species concentration profiles and sulfide growth layer thickness. Lastly, to demonstrate its utility the Goma model was exercised to compute prediction of the average sulfide layer thickness for a couple of hours of sulfidation using realistic transport/kinetic properties and process conditions, and the boundary condition of constant H_2S solute species concentration on the outer non-reacting surface.

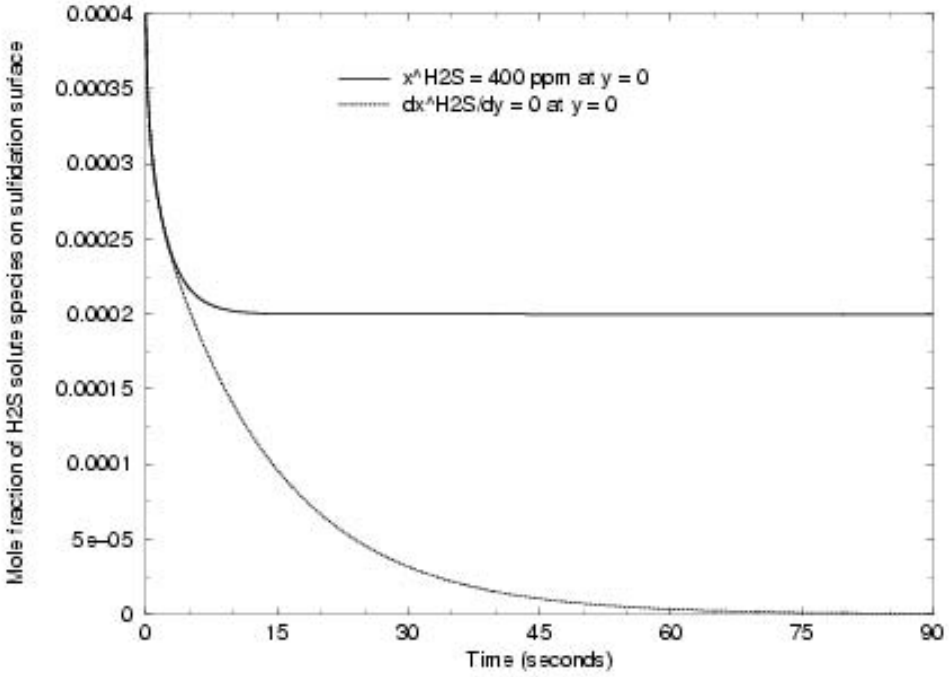

Figure 5a. Effect of boundary condition at the outer non-reacting boundary (y=0) on H_2S solute-species mole fraction on the sulfidation surface. (parameters: D = 0.1 cm^2/s, k = 0.1 cm/s, l = 1 cm, $x_{H_2S,0}$ = 400 ppm; Crank-Nicholson scheme with maximum time step of 0.05 second).

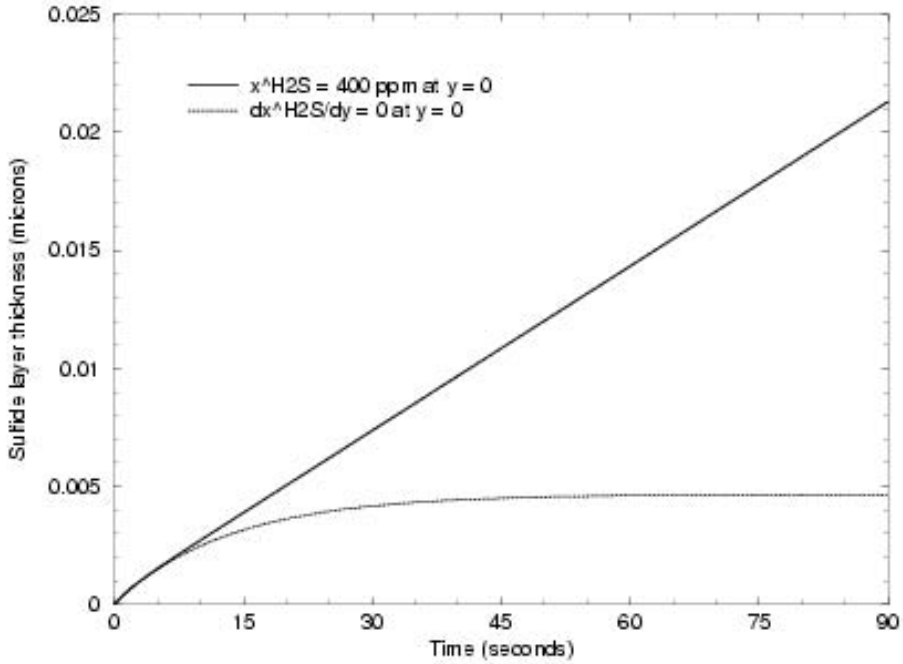

Figure 5b. Effect of boundary condition at the outer non-reacting boundary (y=0) on the average sulfidae thickness. (parameters: D = 0.1 cm^2/s, k = 0.1 cm/s, l = 1 cm, $x_{H_2S,0}$ = 400 ppm; Crank-Nicholson scheme with maximum time step of 0.05 second).

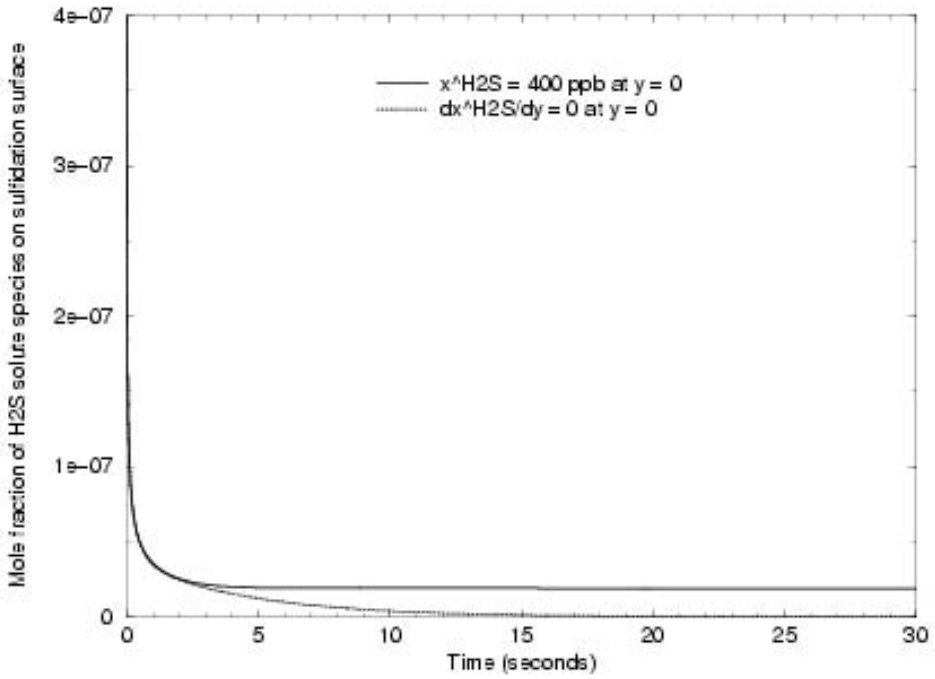

Figure 6a. Effect of boundary condition at the outer non-reacting boundary (y=0) on H_2S solute-species mole fraction on the sulfidation surface. (parameters: D = 0.1 cm^2/s, k = 2 cm/s, l = 1 cm, $x_{H_2S,0}$ = 400 ppb; Crank-Nicholson scheme with maximum time step of 0.005 second).

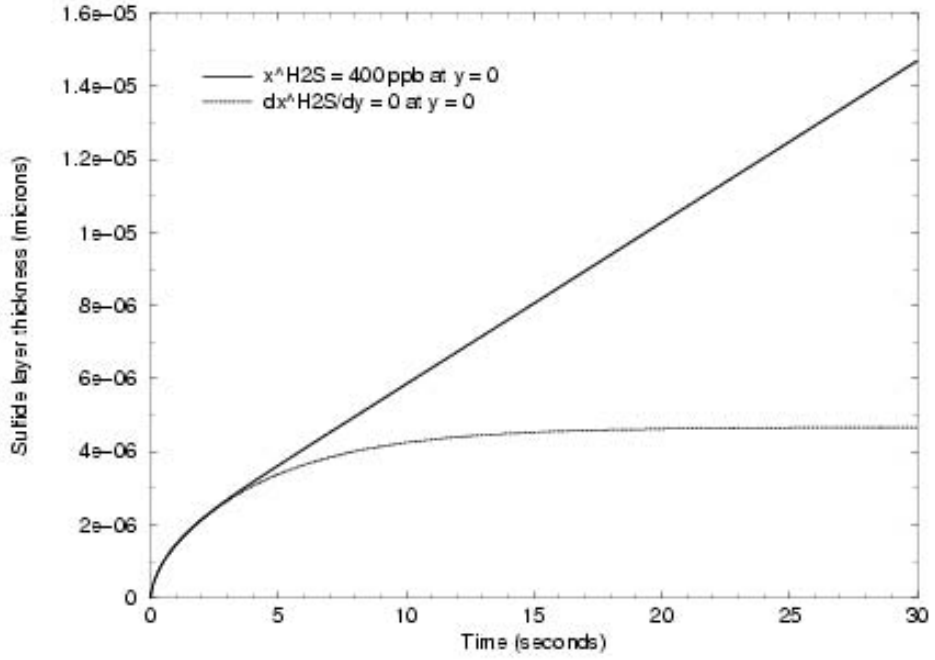

Figure 6b. Effect of boundary condition at the outer non-reacting boundary (y=0) on the average sulfidae thickness. (parameters: D = 0.1 cm^2/s, k = 2 cm/s, l = 1 cm, $x_{H_2S,0}$ = 400 ppb; Crank-Nicholson scheme with maximum time step of 0.005 second).

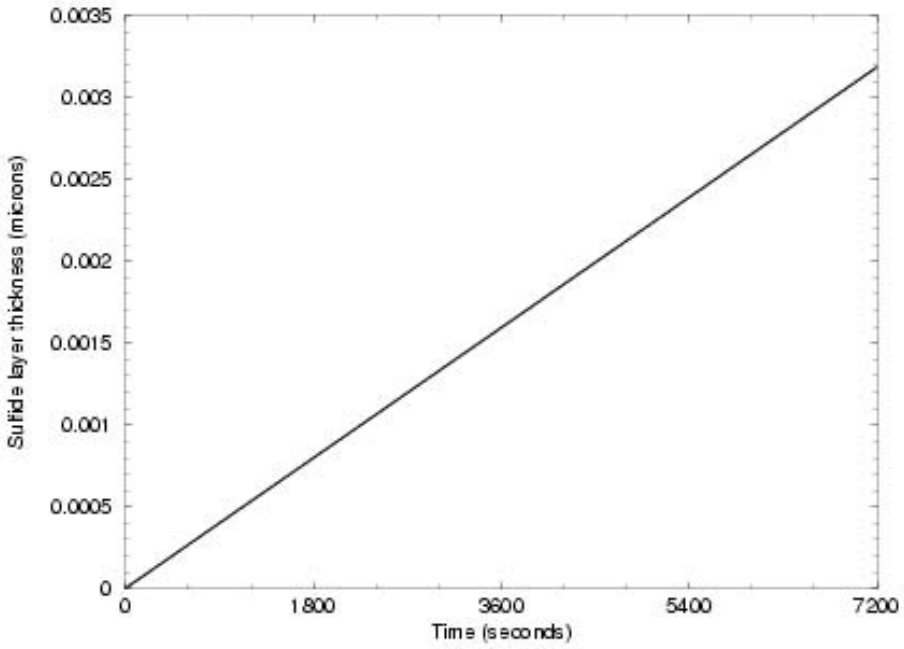

Figure 7. Computed Goma prediction of sulfide layer thickness as a function of time. (parameters: $D = 0.1$ cm^2/s, $k = 2$ cm/s, $l = 1$ cm, $x_{H_2S,0} = 400$ ppb; Crank-Nicholson scheme with maximum time step of 0.005 second).

References

Chen, K. S., "A baseline multi-dimensional mathematical model of copper sulfidation for the initial implementation in Goma", *Sandia Technical Memorandum* dated January 22, 1999.

Chen, K. S., "On the verification of Goma's capability for modeling transient diffusion processes involving dilute solute species and slow surface chemical reaction", *Sandia Technical Memorandum* dated March 31, 2000.

Crank, J., The Mathematics of Diffusion, Second Edition, Oxford University Press, New York, NY (1975).

Larson, R. S., "A physical and mathematical model for the atmospheric sulfidation of copper by hydrogen sulfide", *Sandia Technical Report*, SAND98-8613 (1998).

9. DISTRIBUTION

MS 0384	9140	H. S. Morgan
MS 0825	9110	W. H. Hermina
MS 0834	9112	J. E. Johannes
MS 0827	9113	P. A. Sackinger
MS 0834	9114	J. S. Lash
MS 0834	9114	T. A. Baer
MS 0834	9114	K. S. Chen (5)
MS 0834	9114	H. K. Moffat
MS 0382	9114	P. K. Notz
MS 0834	9114	R. R. Rao
MS 0834	9114	R. A. Roach
MS 0834	9114	P. R. Schunk
MS 0834	9114	A. C.-T. Sun
MS 0889	1861	J. W. Braithwaite
MS 0889	1832	F. D. Wall
MS 0888	1832	D. G. Enos
MS 0889	1832	N. R. Sorensen
MS 1415	1110	J. C. Barbour
MS 1415	1112	N. A. Missert
MS 1415	1112	J. P. Sullivan
MS 0750	6118	L. J. Criscenti
MS 0750	6118	R. T. Cygan
MS 0748	6863	F. Gelbard
MS 9042	8752	C. D. Moen
MS 9042	8752	R. S. Larson
MS 9018	8945-1	Central Technical Files
MS 0899	9616	Technical Library